

1           **Nonlinear carbon feedbacks in CMIP6 and their impacts on future**  
2                           **freshwater availability**

3  
4       Justin S. Mankin<sup>a,b</sup>, Noel Siegert<sup>a,b</sup>, Jason E. Smerdon<sup>b,c</sup>, Benjamin I. Cook<sup>b,d</sup>, Richard  
5       Seager<sup>b</sup>, A. Park Williams<sup>e</sup>, Corey Lesk<sup>a</sup>, Zhiying Li<sup>a</sup>, Harmanveer Singh<sup>a,f</sup>, & Emily  
6                           Martinez<sup>a</sup>

7                           <sup>a</sup> *Department of Geography, Dartmouth College, Hanover, NH*

8                           <sup>b</sup> *Lamont-Doherty Earth Observatory of Columbia University, Palisades, NY*

9                           <sup>c</sup> *Columbia Climate School, Columbia University, New York, NY*

10                          <sup>d</sup> *NASA Goddard Institute for Space Studies, New York, NY*

11                          <sup>e</sup> *Department of Geography, UCLA, Los Angeles, CA*

12                          <sup>f</sup> *School of Marine & Atmospheric Sciences, Stony Brook University, Stony Brook, NY*

13  
14                          *Corresponding author: Justin S. Mankin, [mankin@dartmouth.edu](mailto:mankin@dartmouth.edu)*

15  
16                          \* This work is a preprint, revised for *Journal of Climate*

17  
18  
19  
20  
21  
22  
23  
24  
25  
26  
27  
28  
29  
30  
31  
32  
33  
34  
35  
36  
37  
38  
39  
40  
41  
42  
43  
44  
45  
46  
47  
48  
49

## ABSTRACT

Will plants consume more or less water in a high carbon dioxide [CO<sub>2</sub>] world? What will the hydrologic consequences of those changes will be? Some theories and analyses of earlier generations of Earth System Models (ESM) suggest that transpiration will decline with higher atmospheric carbon dioxide concentrations [CO<sub>2</sub>] due to stomatal closure, thereby enhancing runoff and soil moisture and countering the continental drying predicted by warming alone. We show that the opposite effect prevails in the latest generation of ESMs forced with increasing [CO<sub>2</sub>]: plants themselves contribute to projected soil drying, with smaller effects on runoff, and this picture emerges by considering the interactions between radiatively driven warming and the physiological effects of high [CO<sub>2</sub>] on plants. These interactions act to increase plant-based evapotranspiration (ET) by expanding leaf area and lengthening and warming growing seasons beyond what would be predicted by radiative or biogeochemical effects alone. Collectively, these interactions increase ecosystem water use and dry soils, compensating any land water savings from stomatal closure. At the same time, these interactions have grown and become more uncertain across model generations. We also find that the strength of these plant-water interactions scale with the simulated resilience of the land carbon sink to warming—a key feedback in the carbon cycle. Our results emphasize that a linearity assumption underpinning analyses of carbon, plant, and water interactions is not appropriate for the latest generation of ESMs, with implications for model development, as well as the accurate interpretation of projected changes to the carbon cycle and the consequences for future climate, drought, and water availability.

## SIGNIFICANCE STATEMENT

Understanding plants and how their water use will respond to climate change is essential to understanding future drought and aridity. We demonstrate that interactions between warming and higher atmospheric carbon dioxide in the latest generation of climate models lead to amplified plant growth and associated plant water use. The simulated strength of this interaction is related to weaker land carbon losses from warming. The net result is that in climate models, plant responses forcing enhance land surface drying rather than reduce it, as previous analyses of earlier generations of climate models have found. Our findings highlight that as models become more sophisticated, this leads to a greater ensemble range in carbon feedbacks with implications for how we assess plant influences on water cycle changes.

## 50 1. Introduction

51 Plants and their countervailing responses to anthropogenic greenhouse gas emissions and  
52 climate change will shape the fate of water availability on land (Idso and Brazel 1984). Some  
53 theories, modeling, and nascent observations have suggested that high atmospheric carbon  
54 dioxide concentrations (hereafter [CO<sub>2</sub>]) reduce plant transpiration, leaving more water for  
55 other components of land surface hydrology, like runoff or soil moisture (Idso and Brazel  
56 1984; Swann et al. 2016; Fowler et al. 2019; Roderick et al. 2015; Keenan et al. 2013; Zhou  
57 et al. 2023). Earth System Models (ESMs) parameterize plant photosynthesis to capture the  
58 real world in which carbon gains are optimized while minimizing water losses (Sabot et al.  
59 2022; Medlyn et al. 2011; Cowan and Farquhar 1977; Bonan et al. 2014). As [CO<sub>2</sub>] increases,  
60 stomatal conductance declines (Zhang et al. 2018), diminishing the atmosphere's access to  
61 deep soil moisture via transpiration (Field et al. 1995) and increasing canopy resistance to  
62 evapotranspiration (ET) (Roderick et al. 2015; Milly and Dunne 2016; Lemordant et al.  
63 2018). This leads plants to photosynthesize at a lower water cost under higher [CO<sub>2</sub>],  
64 manifesting as increased plant water use efficiency (WUE) (Keenan et al. 2013; De Kauwe et  
65 al. 2013). Together, such stomatal closure and consequent WUE increases suggest that plant  
66 physiological responses to high [CO<sub>2</sub>] will “turn on the tap” (Jasechko 2018), meaning they  
67 will either directly enhance runoff and soil moisture or reduce the drought and aridity risks  
68 projected by the radiative effects of warming alone (Idso and Brazel 1984; Swann et al. 2016;  
69 Fowler et al. 2019; Roderick et al. 2015; Betts et al. 2007; Milly and Dunne 2016; Yang et al.  
70 2019; Aston 1984; Lemordant et al. 2018; Scheff et al. 2021).

71 While prior work emphasizes that plant responses to [CO<sub>2</sub>] might enhance land water  
72 availability, other analyses emphasize that total plant-based ET increases in the models,  
73 decreasing runoff and soil moisture (Mankin et al. 2018, 2017, 2019), with implications for  
74 drought globally (Cook et al. 2021, 2020). In transient simulations, [CO<sub>2</sub>]-amplified plant  
75 growth due to CO<sub>2</sub> fertilization manifests as increased leaf area (and associated canopy  
76 interception and leaf evaporation). Together with longer and warmer growing seasons, plant-  
77 based ET can increase, even in the face of enhanced stomatal closure. Some studies have  
78 used emergent constraints methods to reduce projection uncertainty in CO<sub>2</sub> fertilization (Cox  
79 et al. 2013; Keenan et al. 2023) and its associated hydrologic consequences (Mankin et al.  
80 2019; Lehner et al. 2019). Yet, persistent uncertainties in plant responses to [CO<sub>2</sub>] across  
81 model generations remain. For example, the IPCC's Working Group I concluded in the 6<sup>th</sup>  
82 Assessment Report that “there is *low confidence* that increased WUE by vegetation will [...]

83 diminish the frequency and severity of soil moisture and streamflow deficits associated with  
84 the radiative effect of higher CO<sub>2</sub> concentrations” (Canadell et al., 2021). The U.S. Fifth  
85 National Climate Assessment differs from the IPCC conclusion, emphasizing that the  
86 remaining uncertainties imply the possibility of plant-induced water savings, stating that “[...]”  
87 changes in plant water use in response to increasing temperatures and rising atmospheric CO<sub>2</sub>  
88 are complex and poorly understood and may either ameliorate or amplify soil moisture and  
89 runoff droughts at the surface” (Leung et al. 2023). As such, this important source of  
90 uncertainty in projections of future freshwater availability, with the potential to inform  
91 drought mitigation and adaptation decisions globally, remains unresolved.

92 The uncertainty in ecohydrological responses to [CO<sub>2</sub>] in models emphasizes the  
93 importance of accurately representing the interactions among the carbon, nutrient, and water  
94 cycles as expressed through plants. Importantly, biogeochemical sophistication in ESMs has  
95 increased considerably across generations (Arora et al. 2020) as land surface models have  
96 rapidly developed (Fisher and Koven 2020). Such model advancements have been driven in  
97 part by the longstanding recognition that simulating coupled carbon and nutrient cycles could  
98 shape nonlinear responses in terrestrial carbon and water budgets. Such responses would  
99 likely shape projected warming and climate impacts as well. For example, there is a long  
100 history of work focused on how nitrogen limitations (Vitousek and Howarth 1991) can cap  
101 plant productivity responses to enhanced [CO<sub>2</sub>], with consequences for carbon feedbacks and  
102 hydrologic impacts (Sokolov et al. 2008; Zaehle et al. 2010; Zaehle 2013; Zaehle et al. 2015;  
103 Thornton et al. 2009; Felzer et al. 2009; Lee et al. 2013; Davies-Barnard et al. 2020).

104 Recent work has shown that the latest generation of ESMs participating in the sixth phase  
105 of the Coupled Model Intercomparison Project (CMIP6) exhibit more sizable interactions  
106 among the radiative and biogeochemical effects of [CO<sub>2</sub>] than in previous CMIP generations,  
107 driven in large part by changes in net primary production (Huang et al. 2022). Here we  
108 extend this important work, showing that in the CMIP6, these interactions in carbon  
109 responses to warming and high [CO<sub>2</sub>] are tied to the carbon-climate feedback and generate  
110 hydrologic responses with implications for the interpretation of how plants responses to  
111 warming and [CO<sub>2</sub>] will shape terrestrial water availability.

112 Using the experiments performed under the CMIP6 Coupled Climate-Carbon Cycle  
113 Intercomparison Project (C4MIP) framework (Jones et al. 2016), we present three key  
114 findings. Firstly, within the CMIP6, there is a sizable interaction between warming and

115 enhanced [CO<sub>2</sub>] that leads to amplified plant growth, the simulated variation in the strength  
116 of which, we show, is tightly associated with variation in the simulated response of the land  
117 carbon sink to warming. Secondly, this amplified plant growth generates an increase in plant-  
118 based ET beyond that predicted by radiative or biogeochemical effects individually or their  
119 sum, cancelling any transpiration reductions from enhanced [CO<sub>2</sub>] and causing relative and  
120 absolute declines in soil water. Lastly, runoff changes within the ensemble are associated  
121 with precipitation changes, not plant-based ET changes. The process-level drivers of  
122 interactive terms in the carbon cycle in CMIP6 relative to earlier CMIP generations is a  
123 crucial question for future evaluation. Together, our results highlight that while CMIP6  
124 projections of future aridity require reconciling plant responses to [CO<sub>2</sub>], doing so provides  
125 little evidence that plant stomatal responses will increase future water availability or offset  
126 radiatively driven drying. Relative to the present day, these idealized projections suggest  
127 increased plant-based ET for much of the globe, with model uncertainties in carbon cycle  
128 responses playing a key role.

129

## 130 **2. Data & Methods**

### 131 *a. Climate model experiments*

132 All ESM data used in this study come from a set of experiments conducted as part of CMIP6  
133 (Jones et al. 2016; Friedlingstein et al. 2006), downloaded from the Earth System Grid  
134 Federation (<https://esgf-node.llnl.gov/search/cmip6/>) and analyzed via Python and R.

135 A common approach to assess whether plants will tend to ‘wet’ or ‘dry’ the surface is to  
136 compare hydrologic responses in a set of idealized ESM experiments that isolate plant  
137 responses to [CO<sub>2</sub>] from other factors associated with radiatively driven changes. This  
138 protocol was originally developed over 20 years ago (Friedlingstein et al., 2006; Fung et al.,  
139 2000) to quantify the strength of carbon feedbacks arising from climate changes versus  
140 enhanced [CO<sub>2</sub>], and is evaluated using the C4MIP framework, a model intercomparison  
141 approved by CMIP6 (Jones et al. 2016). In the idealized experiments used in C4MIP, [CO<sub>2</sub>]  
142 is quadrupled from its pre-industrial level by increasing at a rate of 1% per year for 140 years  
143 (i.e., “4xCO<sub>2</sub>”). The difference among simulations resides in the parts of the model that are  
144 allowed to respond to the [CO<sub>2</sub>] increase. We use data from 13 models (ACCESS-ESM1.5,  
145 BCC-CSM2-MR, CanESM5, CanESM5-CanOE, CESM2, CMCC-ESM2, CNRM-ESM2-1,

146 EC-Earth3-CC, GFDL-ESM4, IPSL-CM6A-LR, MIROC-ES2L, NorESM2-LM, and  
147 UKESM1.0-LL) participating in the experiments that contributed results to C4MIP and for  
148 which the required variables are available: (1) The 1% CO<sub>2</sub> experiment (“1pctCO2”, termed  
149 “coupled” or COU), which is a fully coupled simulation forced with an increase in  
150 atmospheric CO<sub>2</sub> concentrations of 1% per year for 140 years from preindustrial until  
151 quadrupling, conducted as part of the CMIP6 DECK; (2) The 1% [CO<sub>2</sub>] biogeochemical run  
152 (“1pctCO2-bgc”, termed BGC), in which only the land and ocean biogeochemical schemes  
153 respond to [CO<sub>2</sub>], not the climate; and (3) The 1% CO<sub>2</sub> radiatively coupled run (“1pctCO2-  
154 rad”, termed RAD), in which only the radiation scheme responds to increasing [CO<sub>2</sub>], while  
155 the biogeochemical schemes are given preindustrial [CO<sub>2</sub>] levels. Collectively, the COU,  
156 BGC, and RAD experiments allow analyses of how climate and the carbon cycle  
157 independently respond to increased [CO<sub>2</sub>] and how those responses generate carbon  
158 feedbacks from the land and ocean acting to amplify or dampen climate change. We also use  
159 results from seven models that participated in C4MIP during the fifth phase of the Coupled  
160 Model Intercomparison Project (CMIP5) to compare against results from C4MIP for CMIP6  
161 (bcc-csm1-1, CanESM2, CESM1-BGC, HadGEM2-ES, IPSL-CM5A-LR, MPI-ESM-LR,  
162 NorESM1-ME). We note that the net ecosystem exchange variable was not available for  
163 CESM1-BGC from CMIP5; we opted to include the model for all analyses that do not rely on  
164 that variable.

165 Our effort centers on investigating the linearity of carbon and water terms in the C4MIP,  
166 building on earlier work with previous generations of the experiment that focused on their  
167 independent effects in the RAD and BGC runs (Swann et al. 2016; Fowler et al. 2019; Zhou  
168 et al. 2023). Linearity in the context of the C4MIP means that one can generally recover the  
169 fully coupled 1pctCO2 response after the 140-year simulation ( $\Delta\text{COU}$ ) by summing each  
170 model’s isolated biogeochemical ( $\Delta\text{BGC}$ ) and radiative ( $\Delta\text{RAD}$ ) responses as  $\Delta\text{COU} \approx$   
171  $\Delta\text{BGC} + \Delta\text{RAD}$ . Any residual in this calculation,  $\text{NL} = \Delta\text{COU} - (\Delta\text{BGC} + \Delta\text{RAD})$ , is the  
172 “nonlinear term,” NL, for a quantity at hand. We investigate the NL terms for carbon, plant,  
173 and hydrologic variables to assess how the RAD and BGC schemes in the models interact to  
174 shape the COU response and what that implies about how plants shape water availability.

### 175 *b. Data processing*

176 Monthly hydrologic variables (precipitation, “pr”; runoff, “mrro”; transpiration, “tran”; leaf  
177 evaporation “evspsblveg”; soil evaporation, “evspsblsoi”) are converted to monthly totals in

178 mm and then resampled to be water year (WY) totals, which we define as October-September  
179 in the Northern Hemisphere and July-June in the Southern Hemisphere.

180 We preprocess monthly layered soil moisture (“mrsol”) from each model, integrating soil  
181 moisture in each model to a common 2-m depth in units of mm. Soil moisture is analyzed as  
182 a WY average, weighted by the number of days in each month. We also calculate vapor  
183 pressure deficit (VPD, kPa). To do so, we use monthly near-surface (2-m) air temperature  
184 (“tas”) and relative humidity (“hurs”) to estimate the saturation vapor pressure ( $e_s$ , kPa) as  
185  $e_s = 0.61078 \times e^{\frac{17.269T}{273.3+T}}$ , where T is temperature (°C); we calculate VPD as  $vpd = (1 -$   
186  $rh/100) * e_s$ , where rh is relative humidity (%), which we aggregate to WY means.  
187 Ecosystem-scale water use efficiency (WUE) is calculated as the ratio of gross primary  
188 productivity (GPP, “gpp” on ESGF) to transpiration (“tran”). Both of these ratios are  
189 calculated at the WY scale. Extreme precipitation, where analyzed, is calculated using daily  
190 precipitation for the models and experiments for which it is available, estimating the Rx5d  
191 measure, which is the maximum total precipitation (mm) occurring over a five-day period in  
192 each WY. Within each WY, we estimate the start of the growing season using two-day  
193 rolling mean of daily 2-m temperature to identify frost events as those in which two-day  
194 mean temperatures are less than zero. The growing season is then the longest consecutive  
195 stretch of days without frosts in each WY. Throughfall is calculated as the difference between  
196 WY total precipitation and WY leaf evaporation ( $E_L$ ), which is the evaporation of intercepted  
197 precipitation. Gross primary productivity (“gpp”), leaf area index (“lai”), and the land carbon  
198 store quantities (vegetation, “cVeg”; litterfall, “cLitter”; soil, “cSoil”) are all resampled to  
199 WY averages weighting by days per month, as above.

200 In all variables except where otherwise noted, WY changes in response to 4xCO<sub>2</sub> are  
201 calculated as the difference between the average of the last 30 water years and the first 30  
202 water years in each 140-year experiment (e.g., **Figs. S1 and S2**). All quantities are calculated  
203 on the native grids for each model and experiment. Where ensemble means are presented, the  
204 change from each model is calculated and then interpolated to a common 1°x1° grid (based  
205 on the CESM2 grid). For all data except the carbon cycle data, we mask out grid cells where  
206 the ensemble mean climatological monthly peak LAI is below 0.1 m<sup>2</sup>/m<sup>2</sup>. This masks barren  
207 regions like Greenland and the Sahara and other extremely low vegetation areas (shown as  
208 grey in maps). For the ensemble mean fields, statistical significance is calculated at the  
209 regridded grid-point scale based on a Kolmogorov-Smirnov (K-S) test. To do this, we pool all

210 model water years from the first and last 30 years of each experiment and test the statistical  
211 significance of the difference between them. We mask out (in white) any grid cells where the  
212 K-S test indicates little difference between the two periods ( $p \geq 0.05$ ). Where we present  
213 regional or global averages, we area-weight the average of each model on their native grids.

### 214 *c. Carbon cycle feedback calculations*

215 Carbon cycle feedbacks are calculated following previous work using the “BGC-COU”  
216 approach (Arora et al. 2020). Where available, we use the [CO<sub>2</sub>] time series provided by each  
217 model (“co2”) or those provided as a data addendum to Arora et al. (2020) or based on the  
218 last CO<sub>2</sub> value in the preindustrial control simulation. Where CO<sub>2</sub> data are not archived, we  
219 calculate their annual value for year  $i$  assuming a 1% compounding increase from 285 ppm  
220 based on the C4MIP experimental design. Following Arora et al. (2020), for each model and  
221 experiment, we calculate the change in the total global land carbon storage (sum of cVeg,  
222 cLitter, and cSoil in petagrams of carbon PgC) as the area-weighted average of carbon  
223 change at each grid cell. We compute temperature changes based on monthly 2-m  
224 temperature for each model and experiment as the temperature change between year 139 and  
225 year 0 of the simulation.

226 We compute the land carbon-concentration feedback,  $\beta_L$ , or what we call  $\beta$  in this  
227 analysis, as  $\beta = \frac{1}{c'} \left( \frac{\Delta C^* \Delta T' - \Delta C' \Delta T^*}{\Delta T' - \Delta T^*} \right)$ , where  $c$  refers to [CO<sub>2</sub>] change,  $\Delta C$  refers to the change  
228 in total land carbon stores,  $\Delta T$  refers to 2-m temperature changes, primes (‘) refer to  
229 quantities from the control run (COU) and the asterisks (\*) refer to those from the  
230 biogeochemical experiment (BGC); the units of  $\beta$  are PgC ppm<sup>-1</sup>. The carbon-climate  
231 feedback over land, or  $\gamma_L$ , which we call  $\gamma$ , is calculated similarly, as  $\gamma = \frac{\Delta C' - \Delta C^*}{\Delta T' - \Delta T^*}$ ; the units  
232 are PgC °C<sup>-1</sup>. These calculations are performed on global-scale area-weighted average data  
233 over land.

234 To estimate net ecosystem exchange (NEE), we follow earlier work (Huang et al., 2022).  
235 We calculate the “C<sub>int</sub>” quantity they present, which is equivalent to the nonlinear term on net  
236 ecosystem exchange (NEE) or what we call NEE<sub>NL</sub>. We calculate cumulative net primary  
237 productivity (“npp”) and heterotrophic respiration (“rh”) fluxes for each model and grid cell,  
238 estimating the flux in PgC. In contrast to Huang et al. (2022), and to be consistent with the  
239 rest of our analysis, we define the reference carbon flux as the climatological average flux  
240 over the first 30 years of the experiment. We remove the reference flux from the integrated

241 time series in each grid cell, model, and experiment and estimate net ecosystem exchange  
242 (NEE, also called C by Huang et al. (2022)) as the difference between NPP and heterotrophic  
243 respiration; the total change in NEE is simply the value in the last simulation year. We  
244 compute the nonlinear term for NEE, called  $NEE_{NL}$ , as  $NEE_{NL} = \Delta NEE' - (\Delta NEE^* +$   
245  $\Delta NEE^+)$ , where, as above, primes signal the COU, asterisks, the BGC, and the plus sign  
246 (“+”) refers to the RAD simulation. All interactive, or “nonlinear” terms (i.e., COU – BGC –  
247 RAD), which are presented with an “NL” subscript, are calculated similarly as  $X_{NL} = \Delta X' -$   
248  $(\Delta X^* + \Delta X^+)$ . All model-by-model regressions are linear ordinary least squares (OLS) with  
249 the fit and significance (Student’s t-test) reported.

#### 250 *d. Hydrologic budget framework*

251 Following earlier work (Mankin et al. 2018, 2019), we use a hydrologic budget that  
252 assumes climatological WY precipitation (P) is balanced by plant-based ET, or what we term  
253 the “canopy water flux” (C, which is the sum of transpiration and evaporation from the leaf  
254 surface,  $E_L$ ), total runoff (Q, surface and subsurface) fluxes, and soil water (S, which we  
255 calculate as the sum of soil evaporation and each year’s change in WY mean 2-m soil  
256 moisture, calculated as the first difference of the soil moisture time series). Following earlier  
257 work, we write this budget as  $P = C + Q + S$ , where all terms are WY totals in mm. We note  
258 two things: firstly, S can equivalently be represented as the residual of  $P - C - Q$ . In fact, a  
259 comparison between changes in the S term and the change in the residual from  $P - C - Q$  are  
260 similar in pattern and magnitude, suggesting that our S term effectively characterizes the  
261 residual in the hydrologic budget (**Fig. S3**). Secondly, snow is not explicitly considered in our  
262 budget owing to the fact that we analyze climatological WY changes over vegetated regions  
263 (recall the LAI mask described in *b. Data Processing*), making any year-to-year changes in  
264 snowpack exceedingly rare. To ensure this is not an issue and that our budget terms recover  
265 model precipitation, we calculate precipitation partitioning to each WY term C, Q, and S as  
266 the ratio of each to WY total precipitation (e.g., for canopy partitioning as  $C/P$ ). We find that  
267 the partitioning ratios sum to unity nearly everywhere outside of High Mountain Asia,  
268 suggesting the terms we include in our water balance equation capture the scope of each  
269 model’s hydrologic budget and reproduce WY total precipitation.

270 For the regional analyses, we calculate the ensemble mean changes in precipitation  
271 partitioning,  $\Delta(C/P)$ ,  $\Delta(Q/P)$ , and  $\Delta(S/P)$  in the COU for all grid points by averaging across  
272 all models. Based on that ensemble mean response in the COU, we classify and group all grid

273 points that share positively signed changes in partitioning to runoff, known as runoff ratio,  
274  $\Delta(Q/P)$ , or to canopies,  $\Delta(C/P)$ . We then calculate area-weighted averages across all these  
275 grid points for a number of quantities to assess the composite response over regions where  
276 runoff or canopy partitioning increases. We use this same approach to calculate  $\Delta P$  positive  
277 versus  $\Delta P$  negative regions, again, based on the response in the COU. Where time series are  
278 presented, we present the 30-year rolling mean as a function of  $[CO_2]$ ; statistical significance  
279 in the time series is presented as a thicker line where the model signal (the ensemble mean  
280 change evaluated at that time point) is greater than one standard deviation of changes across  
281 the ensemble at that point ( $S/N > 1$ ). Where we present grid-point level scatter plots, we  
282 construct them by pooling all model grid points on their native grids. To calculate the canopy  
283 water flux ( $C$ ) for the ACCESS-ESM1-5 model, we use  $C = ET - \text{soil evaporation}$  (“evspsbl”  
284 minus “evspsblsoi”), as this model does not provide “tran” or “evspsblveg” to the ESGF  
285 archive.

286

### 287 **3. Results**

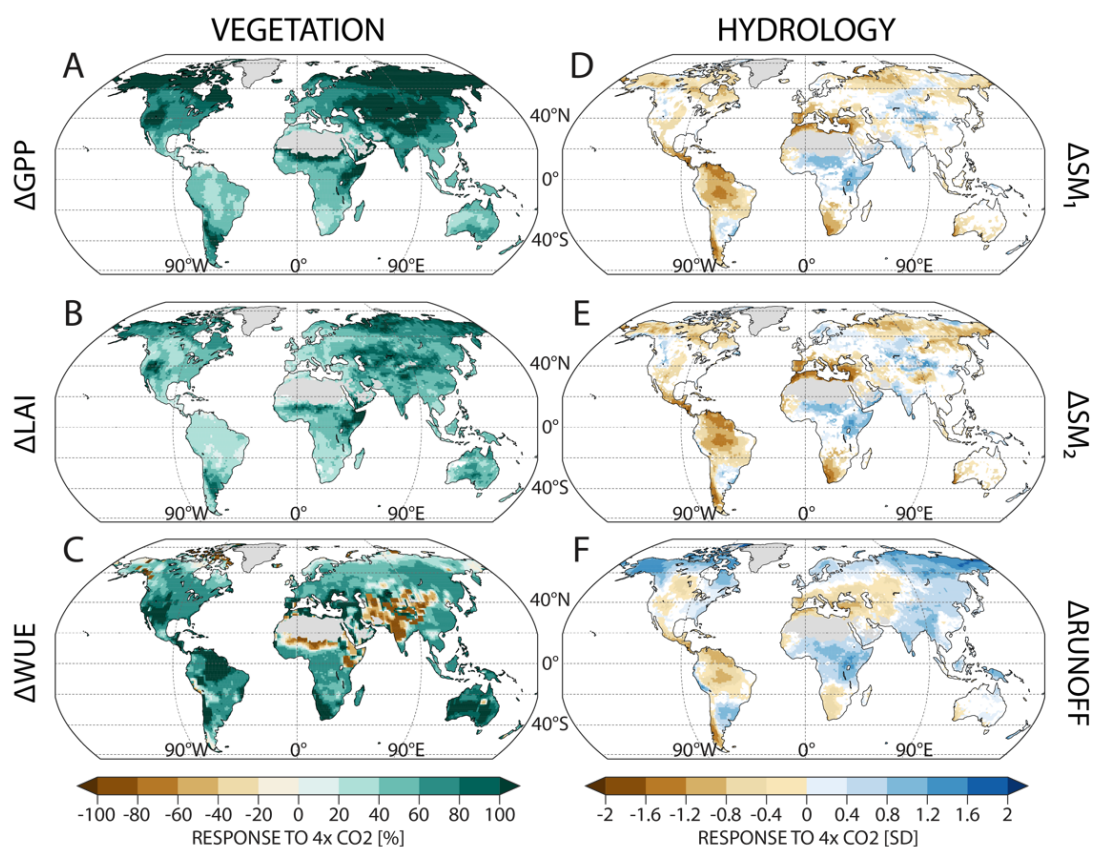
288 Our analysis centers on whether plants will consume more or less water in a high  $[CO_2]$   
289 versus low  $[CO_2]$  world and what the hydrologic consequences of those plant-water use  
290 changes will be. We present our analysis in six parts: (1) we motivate the work by showing  
291 the pattern of projected greening and drying in the CMIP6 ensemble, which suggests future  
292 plant growth and ecosystem health in the face of water availability declines; (2) to understand  
293 this co-located greening and drying, we outline the set of radiative versus physiological plant-  
294 relevant responses in the CMIP6 C4MIP experiments; (3) we show that there are sizable  
295 nonlinear terms in vegetation productivity in the CMIP6 C4MIP experiment, much larger  
296 than those in CMIP5, emphasizing that nonlinear interactions among the RAD and BGC  
297 simulations have grown across model generations and act to amplify projected plant growth  
298 beyond what would be expected from  $CO_2$  fertilization or temperature effects alone; (4) we  
299 show that ensemble variation in nonlinear vegetation growth is closely tied to ensemble  
300 variation in the climate-carbon feedback, or  $\gamma$ , a key climate parameter; (5) we use a simple  
301 hydrologic framework to show that these vegetation growth nonlinearities emerge from  
302 carbon cycle processes and generate positive nonlinearities in plant-based ET; and (6) we  
303 show that these increases in plant-based ET from interactive warming and  $[CO_2]$  are tightly  
304 associated with soil moisture decreases and act to offset water savings from reductions in

305 stomatal conductance in response to high [CO<sub>2</sub>]. Collectively our results trace the  
306 nonlinearity in carbon feedbacks to consequences for vegetation, hydrology, and future water  
307 availability in a high-[CO<sub>2</sub>] world.

308

309 *a. Greening and drying in the CMIP6*

310 The CMIP6 ensemble mean COU simulation shows a consistent spatial pattern of  
311 vegetation “greening” and land surface “drying” implying healthy vegetation in the face of  
312 general reductions in water availability (**Fig. 1**). While the response is consistent with earlier  
313 model generations (Mankin et al. 2017, 2018, 2019), its magnitude appears stronger in the  
314 CMIP6. The most salient indicator of this resides with GPP, which is the rate of plant  
315 photosynthesis (**Fig. 1a, S1**). In the ensemble mean, the fully coupled COU response in WY  
316 GPP is an increase of 68% over global land, reflective of the productivity benefits of  
317 additional [CO<sub>2</sub>] and the strengthening of the land carbon sink (**Fig. 1a, S1**). Complementing  
318 these productivity gains is additional carbon allocation to the leaves of plants, as measured by  
319 LAI, which increases by over 53% in the global mean (**Fig. 1b, S2**). The ensemble-mean  
320 responses in these two quantities, GPP and LAI, share consistent increases with each model  
321 in the COU run, though nuances in the spatial patterns vary (**Fig. S1, S2**). Notably, there is a  
322 57% increase in canopy WUE, suggesting that plants are also more efficient in their water  
323 consumption (**Fig. 1c**). While the ubiquitous signal of the biogeochemical and physiological  
324 effects of [CO<sub>2</sub>] on plants are clearly denoted by the widespread greening in **Figures 1a-c**,  
325 the shared water responses are far more heterogenous. A considerable fraction of land area,  
326 for example, has statistically significant WY drying in 1-m and 2-m soil moisture, as well as  
327 a reduction in WY total runoff (the sum of surface and subsurface runoff in the models). For  
328 example, approximately 50% of land areas have GPP and/or LAI increases collocated with 1-  
329 and 2-m soil moisture declines and about 40% have runoff declines and such greening (**Fig.**  
330 **1d-f**). These results suggest that for many locations, plant growth is unimpeded by regional  
331 land water reductions.



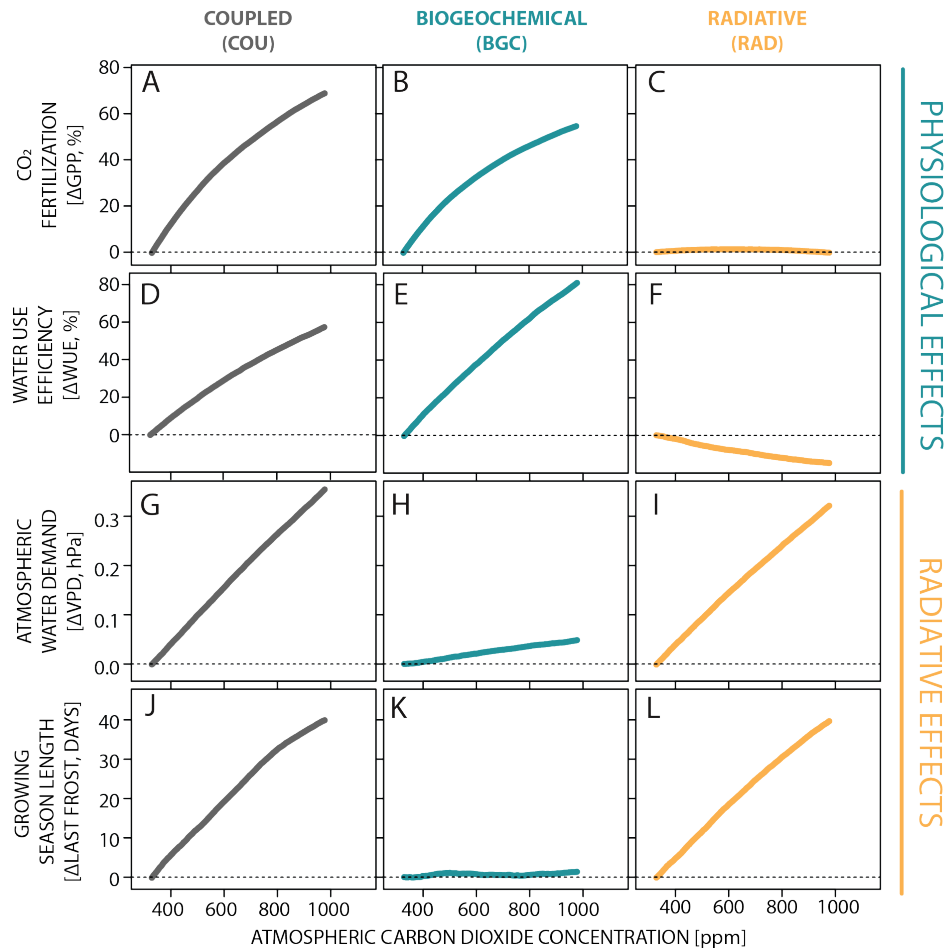
332  
 333 **Fig. 1** Plant greening (in percent change, %) and soil drying (in standard deviations of change, SD) in the  
 334 ensemble mean of the 1pctCO<sub>2</sub> coupled simulation (COU). In response to 4xCO<sub>2</sub> (taken as the  
 335 climatological difference between the last and first 30 WYs of the simulations, **Methods**), we show spatial  
 336 patterns of changes in gross primary productivity, GPP (a), leaf area index, LAI (b), and ecosystem water  
 337 use efficiency, WUE, calculated as the ratio of GPP to transpiration (c), all in percentage (%) changes. We  
 338 also show the hydrologic response in 1-m soil moisture (SM<sub>1</sub>) (d), 2-m soil moisture (SM<sub>2</sub>) (e), and total  
 339 runoff (f), all in standard deviation (SD) changes. Only statistically significant changes are shown  
 340 (**Methods**).

341

342 *b. Plant-relevant responses to high [CO<sub>2</sub>] in the C4MIP experiments*

343 Part of the power of the experimental design of the C4MIP is that it allows us to assess  
 344 why the biogeochemical and radiative responses of plants to enhanced [CO<sub>2</sub>] can result in  
 345 vegetation greening and hydrological drying in the same grid points in the fully coupled COU  
 346 simulations (**Fig. 1**). To illustrate this, we examine the ensemble and global mean responses  
 347 of the physiological and radiative effects of increasing [CO<sub>2</sub>] on terrestrial vegetation across  
 348 the three experiments, COU, BGC, and RAD (**Fig. 2**). As noted in **Section 2a**, comparing the  
 349 BGC and RAD runs (one simulation in which plants are responsive to increasing [CO<sub>2</sub>] and  
 350 one in which they are not) to a third, fully coupled run (COU) in which all parts of the model

351 respond to enhanced  $[\text{CO}_2]$ , allows changes in plant water use and water availability to be  
 352 attributed to radiative (e.g., warming) versus biogeochemical (e.g., plant physiological)  
 353 effects.



354

355 **Fig. 2** Ensemble mean plant-related changes in response to the biogeochemical and radiative effects of  
 356 enhanced  $\text{CO}_2$  concentrations (in parts per million, ppm). For each of the fully-coupled experiment (COU),  
 357 that where the biogeochemical response is isolated (BGC), or that where radiative response is isolated  
 358 (RAD), we show the ensemble-mean global-land fertilization effect, estimated from gross primary  
 359 productivity (GPP, %, **a.-c.**), water use efficiency (WUE, %, **d.-f.**), atmospheric water demand, proxied by  
 360 the vapor pressure deficit (VPD, hPa, **g.-i.**), and the growing season length, proxied by the advance in days  
 361 of the last frost (**j.-l.**).

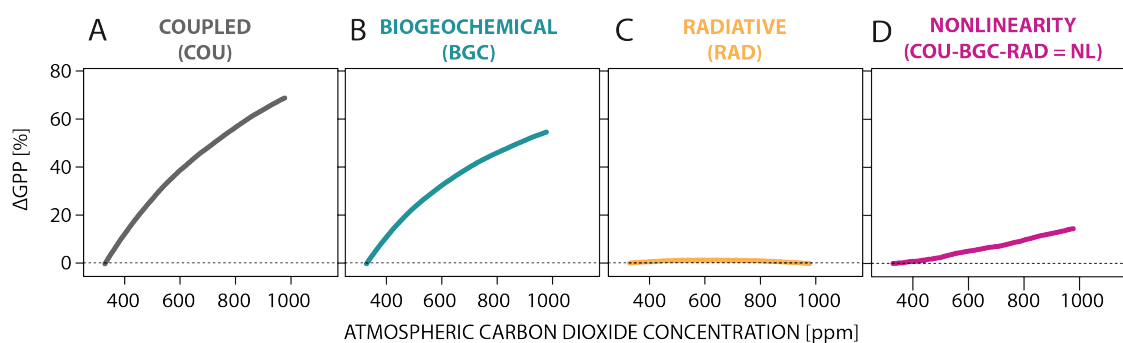
362 The  $\text{CO}_2$ -fertilization effect, as proxied by GPP, prevails in the COU run (**Fig. 2a**) due  
 363 to the strong BGC response (**Fig. 2b**), with no contributions from RAD effects (**Fig. 2c**). Such  
 364 enhanced GPP should tend to increase ecosystem water consumption and dry out the land.  
 365 Stomatal closure under high  $[\text{CO}_2]$  yields increased WUE (**Fig. 2d**) and is considered to be the  
 366 dominant factor contributing to enhanced water availability under anthropogenic forcing,  
 367 particularly when compared to radiative effects alone. In contrast, atmospheric water demand,  
 368 as reflected in VPD (**Fig. 2g**), is driven predominantly by radiative effects (**Fig. 2i**). Plant water

369 consumption would also be shaped by changes to the growing season length, which increase  
370 with forcing due to radiative, rather than biogeochemical, effects (**Fig. 2m-o**).

371

372 *c. Nonlinear interactions between warming and [CO<sub>2</sub>] enhance vegetation growth in CMIP6*

373 Resolving the countervailing physiological and radiative responses presented in **Figure 2**  
374 is critical for appraising whether plants have a net wetting or drying effect under the full  
375 effects of CO<sub>2</sub> forcing. Such an effort, however, is complicated by the potential for nonlinear  
376 interactions among the radiative and biogeochemical effects of CO<sub>2</sub>. Prior work using earlier  
377 generations of C4MIP have assumed that the BGC and RAD effects can be linearly  
378 decomposed, including investigations of how plant responses shape water availability under  
379 high-[CO<sub>2</sub>] (Swann et al. 2016; Fowler et al. 2019; Arora et al. 2020; Zhou et al. 2023);  
380 however, the assumption of linearity in carbon feedbacks does not hold in CMIP6 (Huang et  
381 al. 2022).



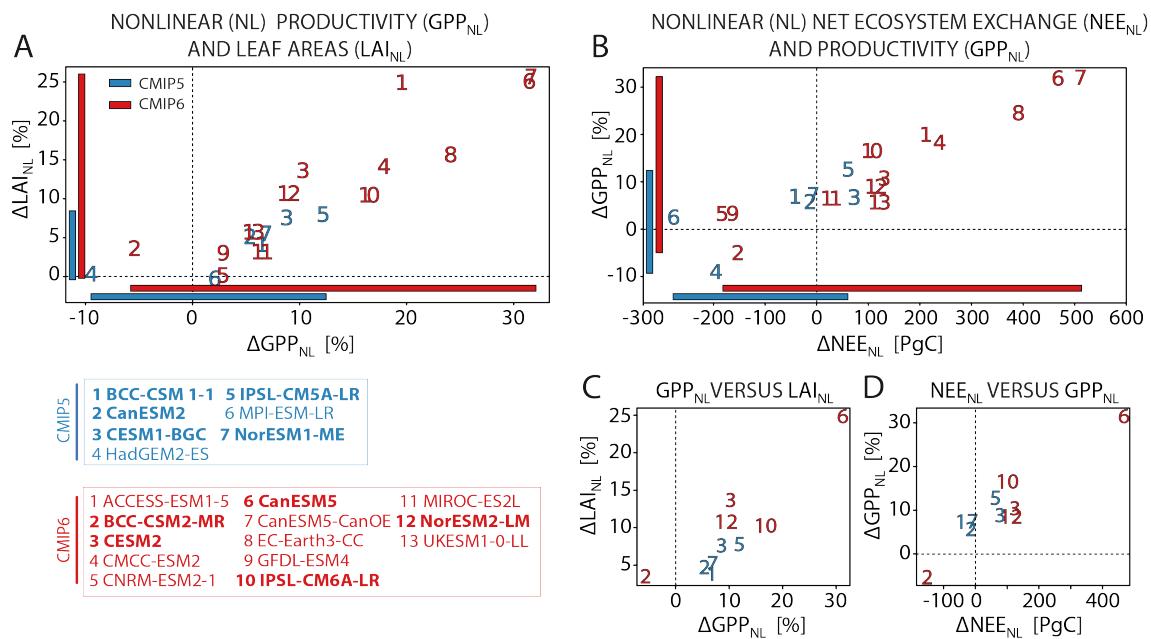
382 **Fig. 3** An emergent nonlinear term in vegetation productivity in the C4MIP **a-d**, The ensemble mean percent  
383 change in gross primary productivity ( $\Delta$ GPP, %) in each of the three experiments, the coupled (COU, **a**), the  
384 biogeochemical (BGC, **b**), the radiative (RAD, **c**), and the nonlinear term (NL, **d**) that is calculated as the  
385 experimental residual all presented as a function of increasing [CO<sub>2</sub>].

386

387 In analyzing the linearity assumption for the CMIP6 C4MIP experiments, there is a large and  
388 significant nonlinear response of enhanced plant growth from the interaction of radiative and  
389 biogeochemical effects of high [CO<sub>2</sub>] (**Fig. 3**). This response can be seen in **Figure 3d**, where  
390 a nonlinear term in GPP, which we term GPP<sub>NL</sub>, increases by ~35% beyond that predicted by  
391 the biogeochemical or radiative effects, or their sum, alone. The magnitude of this nonlinear  
392 GPP term is sizable—it is equivalent to ~25% of the fully coupled COU response in GPP at a  
393 quadrupling of [CO<sub>2</sub>].

394 While such an interaction between  $[\text{CO}_2]$  and warming is expected in the real world, sizable  
395 interactions between RAD and BGC across the ESM ensemble is a new feature in CMIP6.  
396 We can compare the nonlinear plant terms calculated with CMIP6 versus that from an earlier  
397 generation, CMIP5. Nonlinear interactions between the radiative and biogeochemical effects  
398 of high  $[\text{CO}_2]$  on carbon and plants were smaller and less uncertain in CMIP5 than in CMIP6  
399 (**Fig. 4**). Consider for example, the change across generations in  $\text{GPP}_{\text{NL}}$  (**Fig. 4a**). Two  
400 features are worth noting here. First is the expected and tight association between ensemble  
401 variation in  $\text{GPP}_{\text{NL}}$  and  $\text{LAI}_{\text{NL}}$  across both ensembles—positive nonlinear GPP changes imply  
402 positive nonlinear leaf area growth. Second, however, is that the strength of this relationship  
403 and the inter-model variation in the magnitude of these nonlinear terms is considerably larger  
404 in CMIP6 than in CMIP5. The ensemble spread in  $\text{GPP}_{\text{NL}}$  in the CMIP5 spans  $\pm 10\%$ ,  
405 approximately half the range found in CMIP6 (**Fig. 4a**). Moreover, the CMIP5 ensemble  
406 range in  $\text{LAI}_{\text{NL}}$  is less than a third of that for CMIP6 (e.g., compare relative spans of the bars  
407 mapped to the y-axis in **Fig. 4a,b**).

408 The larger uncertainty and magnitude of carbon interactions across model generations  
409 suggests that the assumption that carbon feedbacks can be linearly decomposed into those  
410 arising from biogeochemistry or radiative effects alone, or that any carbon feedback  
411 nonlinearity is trivial does not hold for CMIP6 (**Figs. 3 and 4**). The large nonlinear terms in  
412 GPP presented in **Figure 3** are invariably tied to the carbon cycle and are critical to  
413 understand, particularly given the ongoing efforts to constrain model uncertainty in land  
414 carbon responses to forcing (Hall et al. 2019; Liu et al. 2023; Wenzel et al. 2014). Here we tie  
415 the nonlinear term in GPP to the change in net ecosystem exchange arising from RAD-BGC  
416 interactions,  $\text{NEE}_{\text{NL}}$  (**Fig. 4b**).  $\text{NEE}_{\text{NL}}$  quantity is very tightly correlated with that from  
417  $\text{GPP}_{\text{NL}}$  across both the CMIP5 and CMIP6 ensembles, with a strong positive relationship  
418 consistent across model generations. There is, however, a far larger range of modeled  $\text{NEE}_{\text{NL}}$   
419 values in the CMIP6 than in the CMIP5, suggesting a growing uncertainty in carbon  
420 interactions across generations.



421

422 **Fig. 4** The inter-model association between nonlinear vegetation terms in CMIP5 and CMIP6. We show the  
 423 variation in (a)  $GPP_{NL}$  and  $LAI_{NL}$  and (b) in  $NEE_{NL}$  and  $GPP_{NL}$  in CMIP5 (blue) and CMIP6 (red) for all  
 424 vegetated land areas. The full model range is mapped to each axis via the colored bars. Panels (c) and (d)  
 425 show the same set of results as in (a) and (b) but for the subset of models that are available for both  
 426 generations of CMIP (bolded models in legend): BCC-CSM 1-1 and BCC-CSM2-MR; CESM1-BGC and  
 427 CESM2; CanESM2 and CanESM5; IPSL-CM5A-LR and IPSL-CM6A-LR; NorESM1-ME and NorESM2-  
 428 LM. It is clear that the CMIP6 spans nearly double the range of that from the earlier CMIP5, suggesting a  
 429 growth in uncertainty due to nonlinear interactions among biogeochemistry and warming across generations.

430

431 The growth in RAD-BGC interactions in CMIP6 relative to CMIP5 is perhaps  
 432 expected given the greater representation of terrestrial biogeochemical interactions in the new  
 433 model generation. However, which processes precisely are most important in determining the  
 434 magnitude of the RAD-BGC interaction should be a focus of future work. Hypotheses to test  
 435 could include whether ensemble variation in the representation of nutrient cycles, or other  
 436 factors, such as ecosystem disturbance, succession, and mortality account for the change from  
 437 CMIP5 to CMIP6. It is certainly the case that models are becoming richer in their treatment  
 438 of nitrogen and phosphorous cycles and vegetation cohort dynamics (Fisher and Koven  
 439 2020). As such, a rigorous model-by-model investigation of which key model choices have  
 440 shaped the growing interactions between RAD and BGC changes is essential to better-  
 441 constrain the land carbon sink under warming and its consequences for water and warming.

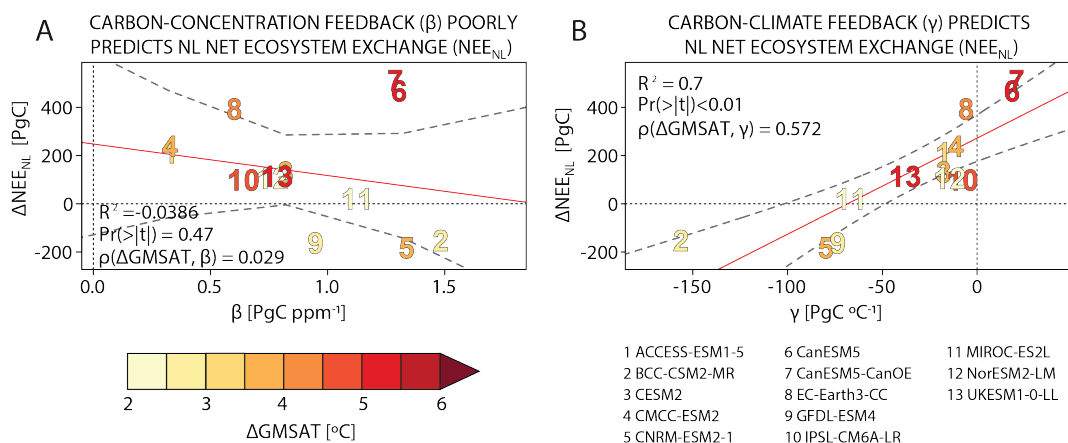
442 At the same time, while increased model sophistication is a possible factor, an expanding  
 443 ensemble range in these nonlinearities could simply be a function of the larger number of

444 models in CMIP6 or the increase in modeling centers contributing simulations. To assess  
 445 whether the growing CMIP uncertainty is robust, we consider the subset of five models that  
 446 have the requisite data available across both generations (**Fig. 4c,d**). The results show that  
 447 even when considering paired models across generations and the same number of models,  
 448 CMIP6 spans a far greater range of nonlinear carbon flux values than CMIP5. All five models  
 449 except those from the Beijing Climate Center (BCC models) show an increase in in LAI<sub>NL</sub>,  
 450 GPP<sub>NL</sub>, and NEE<sub>NL</sub>—some as large as 20 percentage points—as is the case for the Norwegian  
 451 model (NorESM). These results suggest that carbon cycle uncertainty has expanded in the  
 452 CMIP6 relative to the CMIP5, suggesting a potential cost to the increased biogeochemical  
 453 sophistication from an ensemble perspective, even as individual models become more  
 454 accurate or realistic in their treatment of biogeochemistry.

455

456 *d. Nonlinear vegetation growth in CMIP6 tied to carbon feedback parameters*

457 The large nonlinear vegetation response to enhanced [CO<sub>2</sub>] present in CMIP6 models  
 458 (Huang et al. 2022) raises questions about their implications for carbon feedbacks and land  
 459 hydrology. To provide some insights into the former, we extend earlier analyses (e.g., Huang  
 460 et al. (2022)) and examine two key carbon feedback metrics estimated from the C4MIP  
 461 simulations, as detailed in the *Methods* (Arora et al. 2020; Jones et al. 2016): the carbon-  
 462 concentration feedback,  $\beta$ , and the climate-carbon feedback,  $\gamma$ . Positive values of  $\beta$  or  $\gamma$   
 463 indicate land carbon gains in response to increasing [CO<sub>2</sub>] and temperature (**Fig. 5**).



464

465 **Fig. 5** Nonlinear carbon feedbacks and their association with vegetation growth for global land areas in  
 466 CMIP6. **a**, The inter-model association between the nonlinear term in net ecosystem exchange ( $NEE_{NL}$ )  
 467 and the carbon-concentration feedback,  $\beta$ . **b**, The inter-model association between the nonlinear term in net  
 468 ecosystem exchange ( $NEE_{NL}$ ) and the carbon-climate feedback,  $\gamma$ . Colors indicate the magnitude of each  
 469 COU model's 2-m global mean 4xCO<sub>2</sub> surface air temperature (GMSAT) response (land and ocean). The  
 470 13 models included in the analysis are listed. Inset text in each panel indicates the R-squared derived from

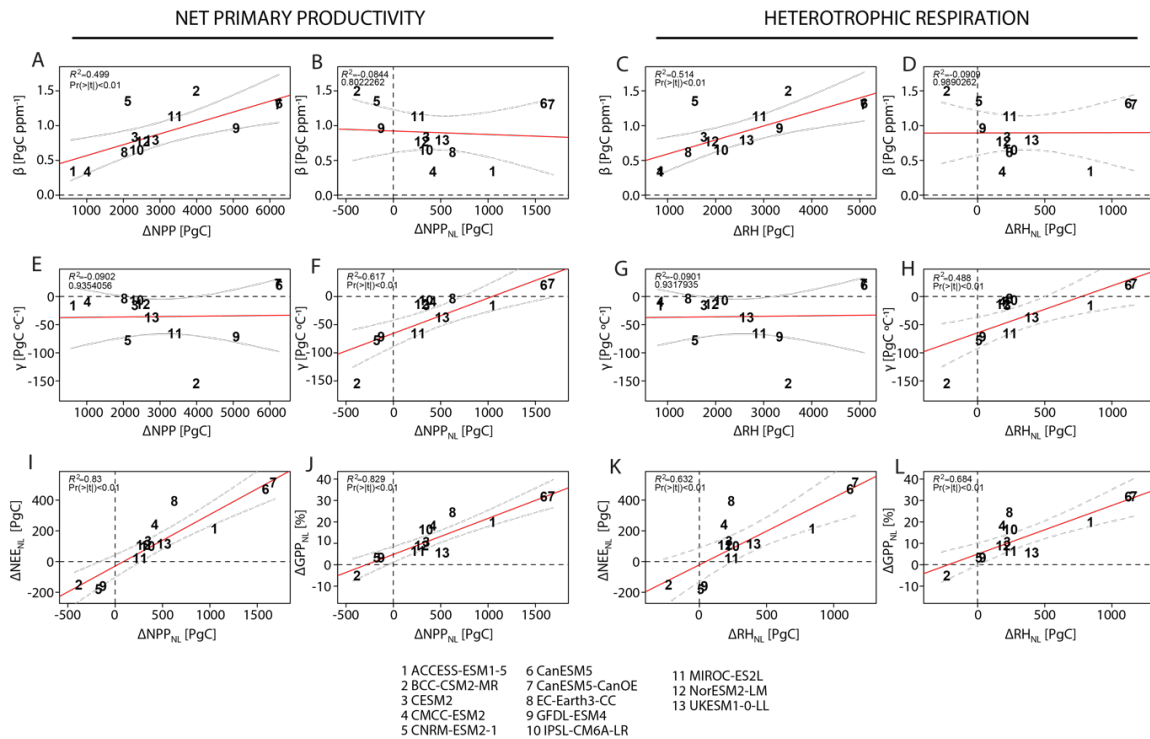
471 a linear regression, shown as a red line, the significance of that regression, and the correlation between the  
472 x- and z-axis variables. Dotted grey lines indicate the 95% prediction-based confidence interval.

473

474 We find that carbon nonlinearities (exemplified by  $NEE_{NL}$ ) scale much more tightly with  
475 model variation in the land-carbon sensitivity to climate ( $\gamma$ , **Fig. 5b**), than to higher  $[CO_2]$   
476 concentrations ( $\beta$ , **Fig. 5a**). In particular, models in which GPP is amplified by the  
477 interactions of warming and  $[CO_2]$  have larger values of  $GPP_{NL}$ , larger values of  $LAI_{NL}$ , and  
478 they also stimulate stronger carbon uptake than release by heterotrophic respiration (a  
479 positive  $NEE_{NL}$ ) relative to models with weaker nonlinear terms (**Fig. 4**). These same models  
480 also tend to be warmer than models with weaker nonlinearities, denoted by the global mean  
481 surface air temperature (GMSAT) changes from the COU in **Figure 5**. As a consequence, the  
482 models with strong nonlinearities in carbon exchange tend to have less negative or even  
483 positive values of  $\gamma$  (**Figs. 5b**). Weaker carbon-climate feedbacks ( $\gamma$ ) imply either stronger  
484 carbon assimilation by the land, less land carbon lost from warming-induced heterotrophic  
485 respiration, or some combination thereof, making for a more resilient land-carbon sink under  
486 climate change (**Fig. 5b**). In contrast, models with smaller  $GPP_{NL}$  have less amplified  $LAI_{NL}$   
487 (**Fig. 4a**), weaker or negative  $NEE_{NL}$  (**Fig. 4b**), less warming (**Fig. 5**) and a more negative  $\gamma$   
488 (from the land perspective), indicating larger land carbon losses to the atmosphere with  
489 warming (**Fig. 5b**).

490 Decomposing NEE into its components, net primary productivity (NPP) and  
491 heterotrophic respiration (RH), confirms the above interpretation and further emphasizes that  
492 these nonlinear carbon terms are more tightly associated with  $\gamma$  than with  $\beta$  (**Fig. 6**).  
493 Cumulative changes in NPP and RH from the COU run, for example, tightly scale with  $\beta$ ,  
494 rather than with  $\gamma$ , (cf. **Fig. 6a,e and c,g**). Such an association is expected and intuitive:  $\beta$  is  
495 dominant in shaping the total carbon cycle response to climate change in the fully coupled  
496 models (Arora et al. 2020). What is notable, however, is that this pattern reverses entirely  
497 when considering nonlinear terms, such as  $NPP_{NL}$  and  $RH_{NL}$  (cf. **Fig. 6b,f and d,h**). Across  
498 the CMIP6 ensemble, the magnitude of  $\gamma$  tightly corresponds with the magnitude of the  
499 RAD-BGC interactions terms in net primary productivity,  $NPP_{NL}$ , and respiration,  $RH_{NL}$

500 (Fig. 6f,h). Both of those terms also shares a tight positive association with  $NEE_{NL}$  and  
 501  $GPP_{NL}$  (Fig. 6i-l).



502

503 **Fig. 6** The CMIP6 inter-model association between the components of NEE,  $NEE_{NL}$  and carbon feedbacks  
 504 for global land areas. We show cumulative changes in net primary productivity, NPP and  $NPP_{NL}$ , left side,  
 505 and heterotrophic respiration, RH and  $RH_{NL}$ , right side, all in of petagrams of carbon (PgC) and carbon  
 506 feedbacks,  $\beta$  (a-d) and  $\gamma$  (e-h) for each model. We also show the model-by-model association between  
 507  $NEE_{NL}$  and  $GPP_{NL}$  and the components that comprise each term (i-l). Ensemble variation in NPP and RH  
 508 changes from the COU are tightly associated with  $\beta$  (a, c) (as opposed to  $\gamma$  (e, g)). However, the nonlinear  
 509 components  $NPP_{NL}$  and  $RH_{NL}$  are not associated with  $\beta$  (b, d). Instead, these nonlinear terms are tightly  
 510 associated with variation in  $\gamma$  (f, h), and are closely related to  $NEE_{NL}$  and  $GPP_{NL}$  (i-l). R-squared values  
 511 and the significance of each regression is shown in the top left of each panel.

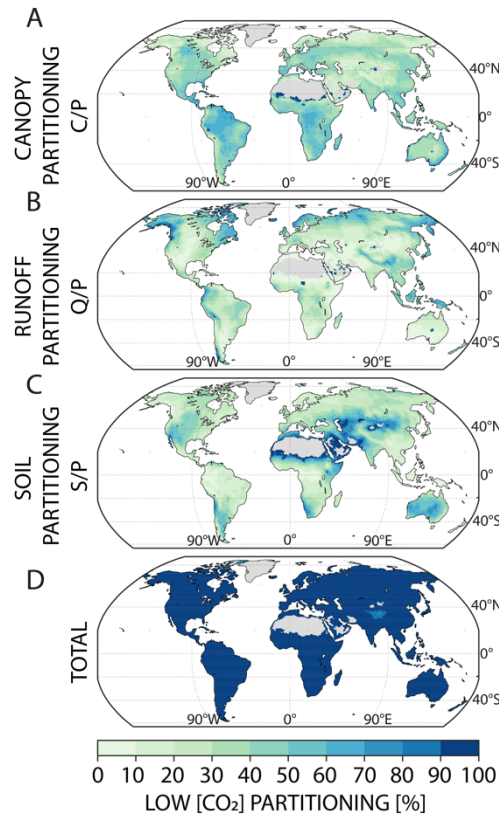
512

### 513 *e. Nonlinear interactions between warming and [CO<sub>2</sub>] enhance plant-based ET*

514 To examine how the nonlinear terms in vegetation growth influence ecosystem water  
 515 use, we use a simple hydrologic budget following earlier work (Mankin et al. 2019, 2018).

516 We analyze changes in how WY precipitation (P) is partitioned at the land surface among  
 517 three terms: the canopy water flux (C), total runoff (Q), and soils (S) (see **Methods**). To  
 518 illustrate that this budget is reasonable and that there is, in fact, closure among the terms, we  
 519 plot the ensemble mean percentage of total WY precipitation going to each term—C, Q, and  
 520 S—in the first 30 years of the COU run (**Fig. 7**). If there is closure, then the sum of the  
 521 partitioning ratios C/P, Q/P, and S/P should approach 100%. We find they do for most

522 regions, save for a small portion of High Mountain Asia (**Fig. 7d**), where multiyear snowpack  
 523 (**Methods**) is present in both observations and models (Gottlieb and Mankin 2024).



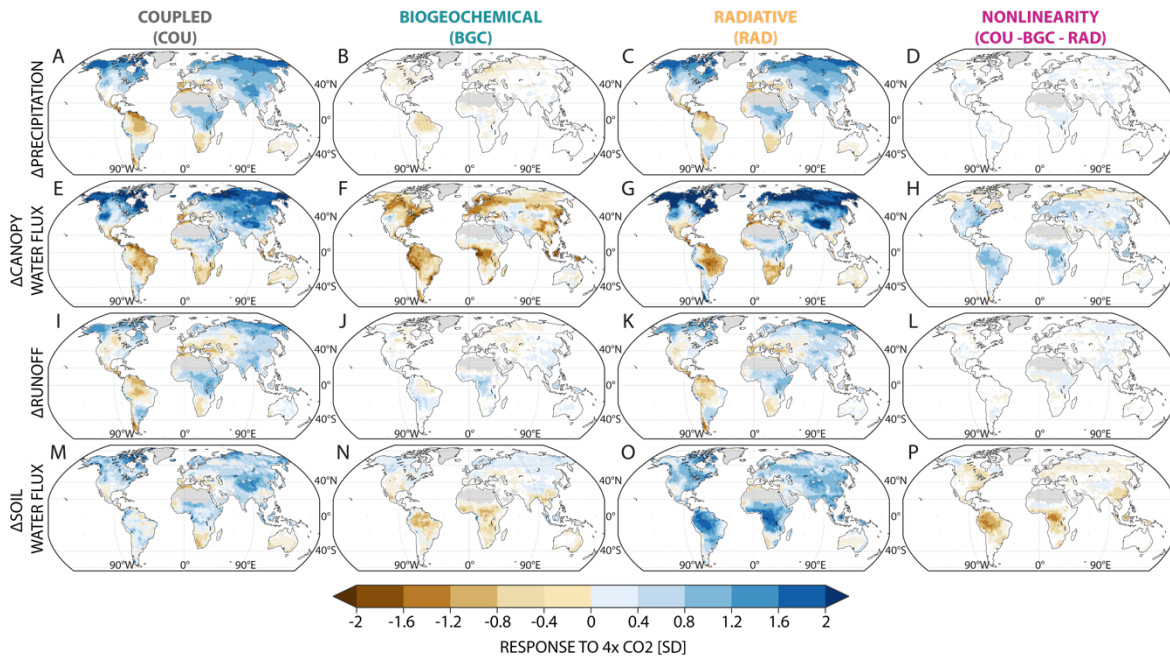
524

525 **Fig. 7** Ensemble mean precipitation partitioning during the first 30 years of the 1pctCO<sub>2</sub> (COU) simulation  
 526 expressed as a percent (rather than fraction) for the canopy (C/P) (**a**), runoff (Q/P), (**a**), and soils (S/P), (**c**).  
 527 The sum of the three ratios (**d**) should approach 100% assuming that at climatological WY scales as  
 528  $P=C+Q+S$ .

529

530 Maps of total changes in WY hydrologic variables (**Fig. 8**) and their relative changes  
 531 from precipitation partitioning (**Fig. 9**) show that nonlinear terms increase plant-based ET  
 532 both relatively (as a fraction of precipitation) and absolutely (in standard deviations of  
 533 change) in response to high [CO<sub>2</sub>]. As expected, and consistent with the pattern of the fully  
 534 coupled ensemble mean response to forcing, precipitation in the COU increases in the  
 535 extratropical northern latitudes and equatorial Africa and Asia, with drying in the  
 536 Mediterranean, the Amazon, Central America, southern Africa and Chile, and uncertain  
 537 change elsewhere (**Fig. 8a**). Across most of the budget terms, P (**Fig. 8a-d**), C (**Fig. 8e-h**), Q  
 538 (**Fig. 8i-l**), and S (**Fig. 8m-p**), the ensemble mean pattern in the COU is primarily driven by  
 539 the forced climate response in the RAD, more so than the BGC or NL terms, which are  
 540 modest in the ensemble mean, if and where they are significant. This response is because P

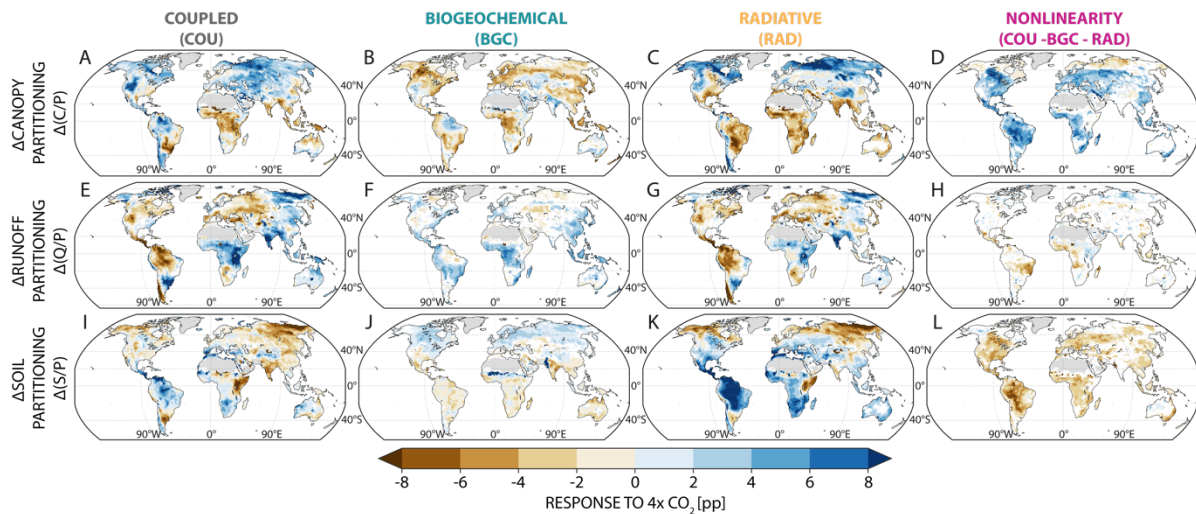
541 changes are driven by the thermodynamic response in the RAD, whereas forced P responses  
 542 in the BGC are smaller (though still potentially important) (Skinner et al. 2017).



543  
 544 **Fig. 8** Hydrologic changes across experiments under the water budget of  $P = C + Q + S$ , presented in standard  
 545 deviations of change (SD) in response to  $4\times\text{CO}_2$ . The ensemble mean response of precipitation (**a-d**), canopy  
 546 water flux,  $C$  (**e-h**) total runoff ( $Q$ , **i-l**), and soils (change in 2-m soil moisture storage plus soil evaporation,  
 547 **Methods, m-p**) in the fully coupled experiment (COU), the experiments in which the biogeochemical response  
 548 is isolated (BGC), the radiative response is isolated (RAD), and the residual or nonlinear interaction between the  
 549 RAD and BGC (calculated as  $\text{COU}-\text{BGC}-\text{RAD}$ ). Gray regions indicate where historical peak leaf area index is  
 550 below 0.1. Only statistically significant changes (K-S test,  $p < 0.05$ ) are shown and all maps are at the WY scale.  
 551

552 Beyond the pattern of precipitation changes, the stomatal response from higher  $[\text{CO}_2]$  in  
 553 the BGC run clearly leads to a global-scale reduction in plant-based ET, the  $C$  term in our  
 554 budget (**Fig. 8f**). The ubiquity of the brown contours in **Figure 8f** is striking, and it is this  
 555 response in the C4MIP BGC that gives rise to the suggestion that plant physiological  
 556 responses to enhanced  $[\text{CO}_2]$  will tend to enhance water availability for soils or rivers,  
 557 offsetting the drying from RAD effects or  $\text{CO}_2$  fertilization. However, the NL term for plant-  
 558 based ET,  $C_{\text{NL}}$  (**Fig. 8h**), shows a pattern of *increases* that roughly mirrors the *reductions* in  
 559 plant-based ET in the BGC run (**Fig. 8f**). This means that nonlinear interactions between the  
 560 radiative and biogeochemical effects cancel any plant-water savings from the BGC run,

561 leaving the RAD run to dominate the COU pattern. It is also noteworthy that there are  
 562 decreases in the  $S_{NL}$  term (**Fig. 8p**), which we explore further in later sections.  
 563

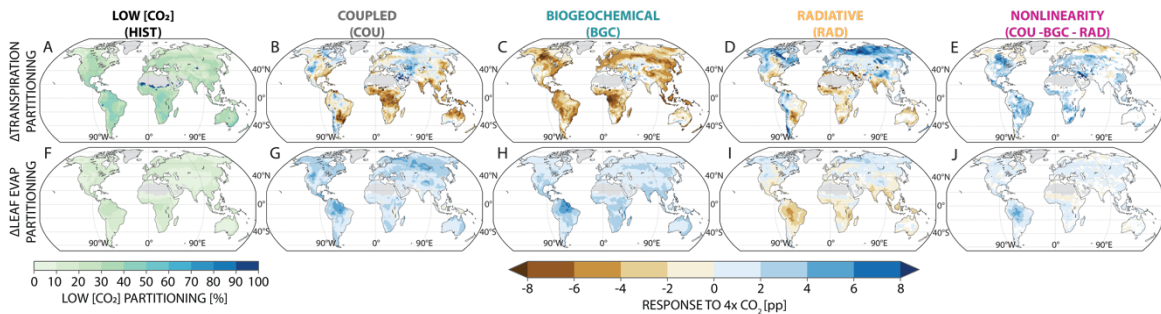


564  
 565 **Fig. 9** Changes in WY precipitation partitioning at the land surface to each term in the hydrologic budget  
 566 in response to 4xCO<sub>2</sub>, presented in percentage points (pp) of change. For each experiment and the NL term  
 567 (columns) we show the spatial pattern of changes in the fraction of total WY precipitation directed to  
 568 canopies,  $\Delta(C/P)$  (**a-d**), runoff,  $\Delta(Q/P)$  (**e-h**), and soils,  $\Delta(S/P)$  (**i-l**) (see **Methods**). Gray regions indicate  
 569 where historical peak leaf area index is below 0.1. Only statistically significant epoch changes (K-S test,  
 570  $p < 0.05$ ) are shown.  
 571

572 The nonlinear terms are robust in the parts of land hydrology most closely associated with  
 573 vegetation; this pattern also persists when we examine relative changes in precipitation  
 574 partitioning. The maps in **Figure 9** show the change in the fraction of WY precipitation  
 575 allocated to each hydrologic budget term, C, Q, and S. In the fully coupled COU run, the  
 576 change in precipitation partitioning to plant canopies,  $\Delta(C/P)$ , increases across vast swaths of  
 577 the globe, particularly in the northern and eastern hemispheres (**Fig. 9a**) as plants in those  
 578 regions demand larger fractions of each drop of precipitation. In tropical Africa and Asia,  
 579 canopy partitioning declines (**Fig. 9a**), likely due to WUE and stomatal closure effects being  
 580 stronger than CO<sub>2</sub> fertilization in the BGC runs (**Fig. 9b**) and because of either reduced  
 581 precipitation or higher VPD in the RAD runs (**Fig. 9c**). Changes in runoff partitioning,  
 582  $\Delta(Q/P)$ , often called runoff efficiency or runoff ratio, show declines over much of the  
 583 northern and eastern hemispheres (**Fig. 9e**), driven predominantly by radiative warming (**Fig.**  
 584 **9g**), and show increases in tropical Africa and Asia through contributions from both the  
 585 biogeochemical and radiative effects of increasing [CO<sub>2</sub>]. The BGC contribution to increased  
 586 Q/P and decreased C/P (cf. **Fig. 8b, f** and **Fig. 9b, f**) is the “plants turn on the tap” response

587 (Jasechko 2018), where stomatal closure and WUE increases spare water for runoff and or  
 588 soils. Lastly, there are the changes in precipitation partitioning to soil water flux,  $\Delta(S/P)$  (**Fig.**  
 589 **9i-k**), which outside of western North America, shows an inverse pattern to runoff  
 590 partitioning (cf. **Fig. 9e, i**) driven largely by radiative effects (**Fig. 9k**). Because the  
 591 partitioning ratios sum to unity (**Fig. 7**), changes are bounded such that increases in one term  
 592 must be compensated by decreases in another.

593 Importantly, changes in precipitation partitioning at the land surface for the COU run do  
 594 not equal the sum of changes in the BGC and RAD components. A large, positive, and  
 595 statistically significant  $(C/P)_{NL}$  spans most regions globally in the C4MIP (**Fig. 9d**), a feature  
 596 that is associated with decreased  $(Q/P)_{NL}$  and, primarily,  $(S/P)_{NL}$  (**Fig. 9h and I**). Increases in  
 597  $\Delta(C/P)_{NL}$  shown in **Figure 9d** arise from some combination of changes in transpiration and  
 598 leaf evaporation, which are combined in the C term (**Methods**).



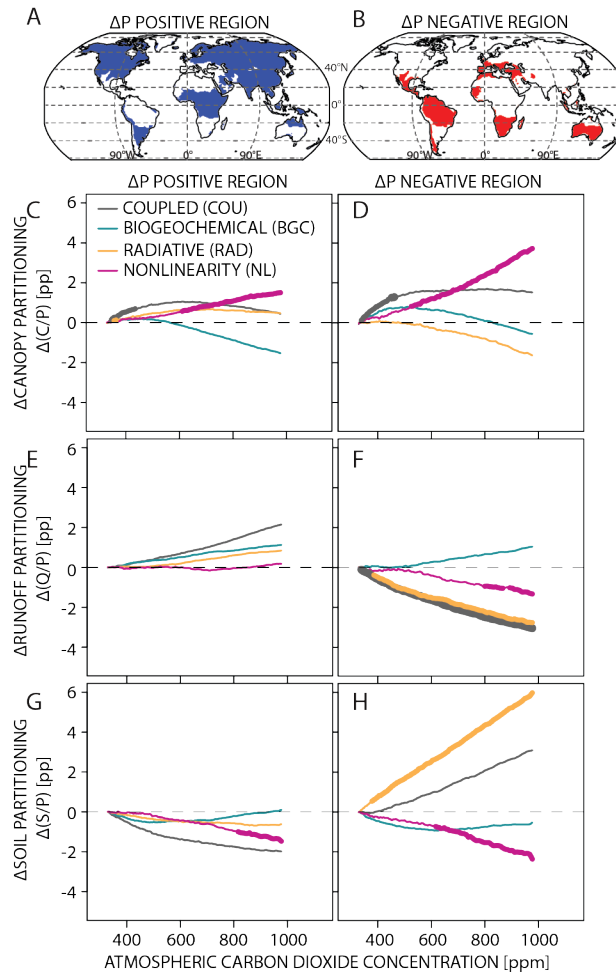
599 **Fig. 10** WY precipitation partitioning and its changes across experiments to the components of plant-  
 600 based ET in percentage points of change (pp). The ensemble mean low  $[CO_2]$  partitioning, defined as the  
 601 first 30 years of the 1pctCO<sub>2</sub> (COU) run (first column, **a,f**) and then its change in the COU (second  
 602 column, **b,g**), BGC (third column, **c,h**), RAD (fourth column, **d,i**) simulations, and then in the NL term  
 603 (fifth column, **e,j**). We show the response for transpiration partitioning (first row **b-e**, calculated as WY  
 604 changes,  $\Delta(TRAN/P)$ ) and leaf evaporation partitioning (second row, **g-j**, calculated as  $\Delta(E_L/P)$ ).  
 605  
 606

607 To examine the independent changes, we decompose the partitioning of precipitation in  
 608 the C term in **Figure 10**. It is clear that positive  $(C/P)_{NL}$  changes are driven by nonlinear  
 609 increases in precipitation partitioning to transpiration, though important contributions also  
 610 come from increased canopy evaporation (**Fig. 10e, j**). In other words, while BGC responses  
 611 alone are associated with plant responses that diminish transpiration and thus spare water for  
 612 runoff and soil moisture (cf. **Fig. 9b, f, j**), that alone does not shape plant-based ET changes.  
 613 Nonlinear interactions between BGC and RAD responses favor relative increases in plant-  
 614 based ET to the sacrifice of runoff and soil moisture when controlling for precipitation  
 615 changes (cf. **Fig. 9d,h,I**), predominantly by enhancing transpiration (**Fig. 10e**). The  
 616 consequence of RAD and BGC interactions is an increase in plant-based ET relatively and

617 absolutely, reducing soil water (**Figs. 10p and 9l**), and to a lesser extent, runoff ratio (**Fig.**  
618 **9h**).

619 It is notable that this nonlinear increase in relative plant water use is insensitive to the  
620 sign of precipitation change (**Fig. 11**). To make this assessment, we divide global grid points  
621 into regions where precipitation increases versus where it decreases based on COU response  
622 (**Fig. 11a,b, Methods**). For each of these domains, we present the area-weighted average  
623 response as a function of  $[\text{CO}_2]$  in each experiment as well as the NL term (**Fig. 11c-h**).  
624 Regardless of the precipitation change, there is a significant increase in precipitation that is  
625 partitioned to plants from the nonlinear interactions between the radiative and  
626 biogeochemical effects of  $[\text{CO}_2]$  (**Fig. 11c,d**, bolded pink lines). It is also interesting that in  
627 regions with decreased precipitation, there is a significant decrease in runoff ratio from the  
628 NL term that emerges under high  $[\text{CO}_2]$ , countering any increase in runoff partitioning from  
629 the BGC (cf. the pink and green lines in **Fig. 11f**). There is essentially no significant  
630 contribution of enhanced runoff ratio in precipitation positive regions (**Fig. 11e**), suggesting  
631 that average WY precipitation increases alone are insufficient to increase runoff efficiencies.  
632 Instead, we find that it is increases in extreme precipitation that are key to increasing runoff  
633 ratio (**Fig. S4**).

634 Regardless of the precipitation change, the NL term acts to decrease precipitation  
635 partitioning to soils, denoted by the significantly declining pink lines (**Fig. 11g,h**).  
636 Nevertheless, the direction of precipitation change appears to shape the extent to which  
637 runoff efficiency or soil partitioning is affected, with precipitation decreases leading to an  
638 increase in nonlinear partitioning to plants  $(C/P)_{\text{NL}}$  (pink line in **Fig. 11d**), and a decrease in  
639 nonlinear partitioning to runoff  $(Q/P)_{\text{NL}}$  and soils  $(S/P)_{\text{NL}}$  (pink lines in **Fig. 11f**, and **h**,  
640 respectively). Together, these results indicate that the NL increase in plant-based ET occurs  
641 regardless of precipitation change and can diminish water partitioning to soils and runoff.  
642 This response occurs in spite of enhanced WUE and surface resistance to ET that are thought  
643 to be key to runoff enhancement or drought-risk reductions (Roderick et al. 2015; Swann et  
644 al. 2016; Fowler et al. 2019). Where canopy partitioning does decrease, such as from the  
645 BGC effect (insignificant green lines in **Fig. 11c,d**), the nonlinear term acts to weaken or  
646 completely counter that effect (significant pink lines in **Fig. 11c,d**).

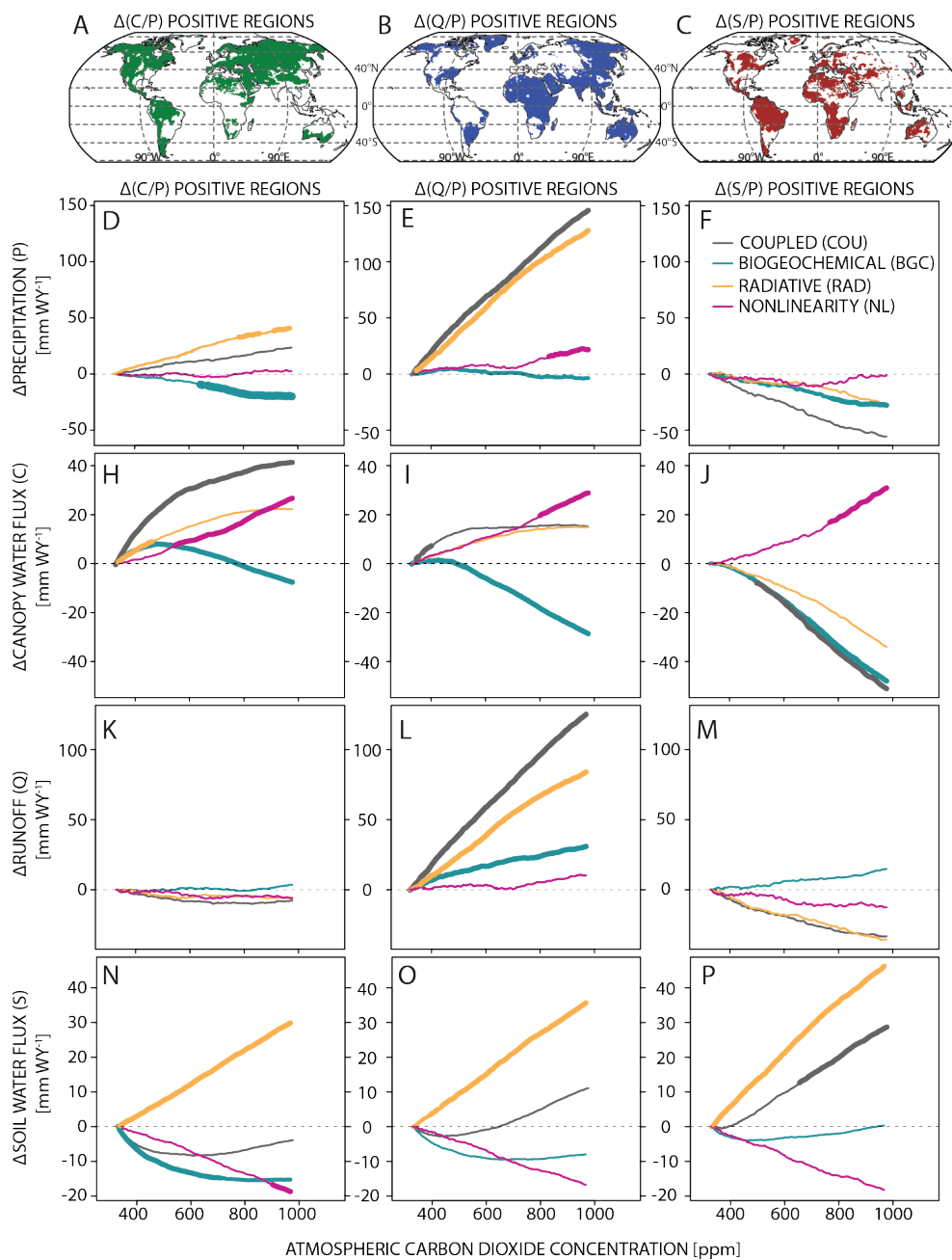


647

648 **Fig. 11** Precipitation partitioning responses in percentage point change (pp) to increasing [CO<sub>2</sub>] in ppm.  
 649 Maps show the regions of ensemble mean precipitation increases in blue (a) and decreases in red (b) from  
 650 the COU run. These maps define the domains over which we evaluate the ensemble mean changes in each  
 651 experiment for each quantity presented in panels c-h. The ensemble mean area-weighted regional average  
 652 responses in percentage points [pp] of canopy partitioning, C/P (c-d), runoff partitioning, Q/P (e-f), and  
 653 soil partitioning S/P (g-h) in precipitation increasing (a) and decreasing (b) regions as a function of [CO<sub>2</sub>].  
 654 Ensemble statistical significance is presented as a bolded line (Methods).

655 The changes in precipitation partitioning from nonlinear interactions between the RAD  
 656 and BGC runs generate wide changes in land hydrology. To illustrate the connection between  
 657 the relative changes presented in Figures 9-11 and the changes presented in Figure 8, we  
 658 divide global land areas into three regions, one in which ensemble mean COU changes in  
 659 canopy partitioning are positive (called “Δ(C/P) positive region”), one in which changes in  
 660 runoff partitioning are positive (or “Δ(Q/P) positive region”), and one in which changes in  
 661 soil partitioning are positive (or “Δ(S/P) positive region”) (Fig. 12a-c, S4). We note two  
 662 revealing patterns of hydrologic change: Firstly, the precipitation increase in the Δ(Q/P)  
 663 positive region is far larger than in the Δ(C/P) positive region, as precipitation changes have a

664 first-order control on enhancing runoff ratio and total runoff, even in the BGC run (cf. **Fig.**  
 665 **12d and e** with **Fig. 12k and l**).



666  
 667 **Fig. 12** Total hydrologic changes in mm per WY across experiments and the nonlinear terms in response to  
 668 increasing  $[CO_2]$  in ppm. Maps (a-c) of regions where the ensemble mean partitioning increases for  
 669  $\Delta(C/P)$ ,  $\Delta(Q/P)$ , and  $\Delta(S/P)$ , based on the COU 4xCO<sub>2</sub> response (see maps in **Fig. 9, a, e, i**). The maps in  
 670 (a-c) define the domains over which we evaluate the ensemble mean change in total hydrologic quantities  
 671 in mm per WY presented in panels d-p, linking how the partitioning changes shape total changes in C, Q,  
 672 and S. For each partitioning increase region, we show the time series of ensemble mean precipitation  
 673 changes (d-f), canopy water flux, C, changes (h-j), runoff, Q, changes (k-m) and soil water, S, changes (n-

674 p) in each experiment and the nonlinear term. Ensemble statistical significance in the time series is  
675 presented as a bolded line (**Methods**).

676

677 The  $\Delta(S/P)$  positive regions contrast with the  $\Delta(C/P)$  and  $\Delta(Q/P)$  positive regions in  
678 that they have no statistically significant change in precipitation in the COU run (**Figure 12f**).  
679 Secondly, and consistent with the nonlinear term in carbon and in plant-based ET, our results  
680 also demonstrate a clear—and previously unaccounted for—significant nonlinear increase in  
681 the canopy water flux, C (and its components: transpiration and leaf evaporation), regardless  
682 of the partitioning region (bolded pink lines in **Fig. 12h-j**). Such ubiquity suggests that the  
683 nonlinear term in canopy partitioning, or  $\Delta(C/P)_{NL}$ , is associated with a positive nonlinear  
684 term in the absolute plant-based ET ( $\Delta C_{NL}$ ) as well, regardless of whether canopy partitioning  
685 increases in the COU run. These changes are sizable, amounting to more than 50% of the  
686 canopy water flux response in the COU experiment. The widespread increase in plant-based  
687 ET from interactions between BGC and RAD runs cancel or exceed any water savings that  
688 accrue in the BGC runs from stomatal closure in the CMIP6 across precipitation changes  
689 (**Fig. 11**), or hydrologic partitioning changes (**Fig. 12**).

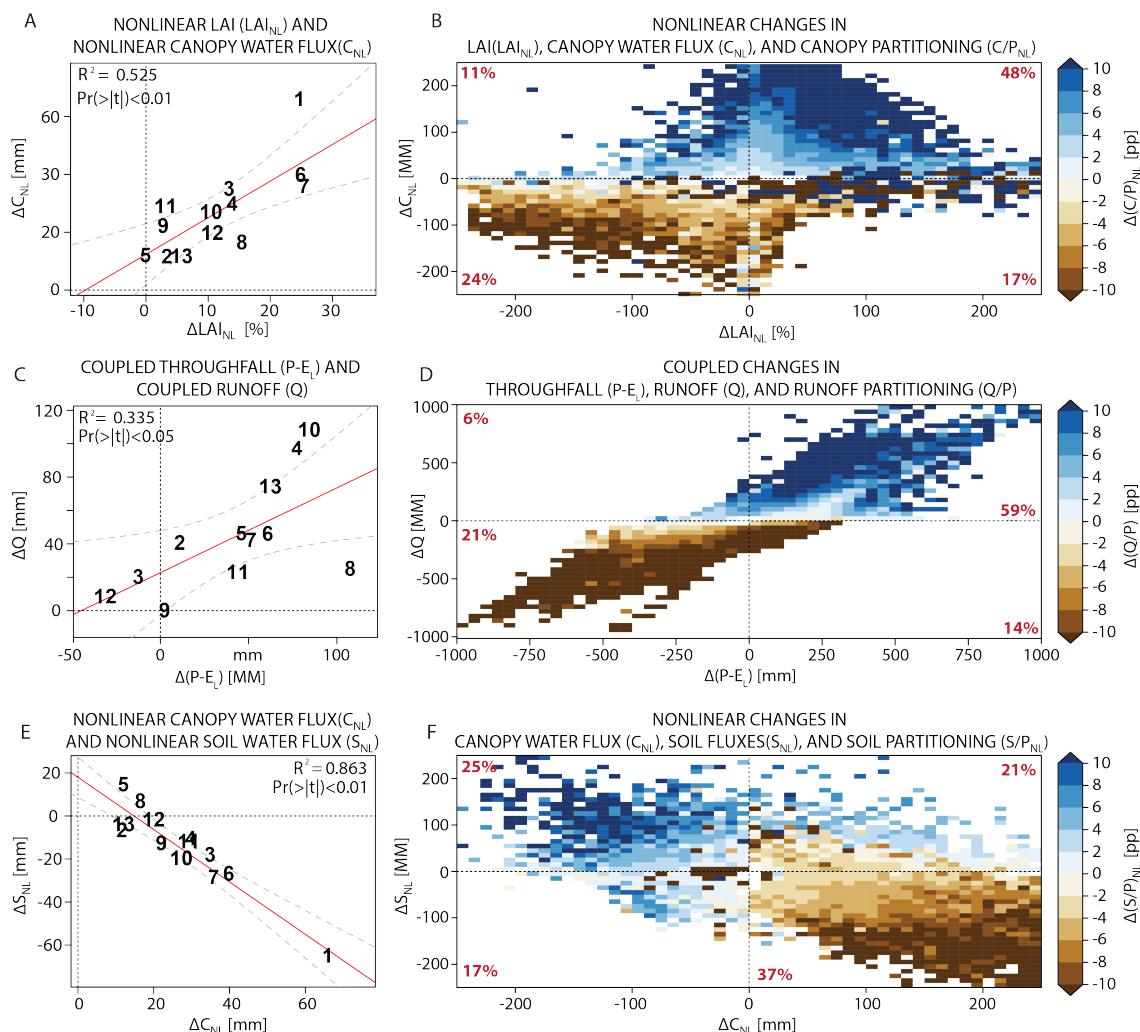
690

691 *Nonlinear plant-based ET reduces soil moisture while runoff is controlled by precipitation*

692 To connect our two sets of results—the nonlinear vegetation growth from carbon  
693 feedbacks (**Fig. 3-6**) and the nonlinear hydrologic changes (**Figs. 8-12**)—we examine inter-  
694 model global changes in C, Q, and S, as well as their grid-point responses to evaluate  
695 whether they are consistent across model spatial scales (**Fig. 13**).

696 At the global scale, and across the C4MIP ensemble, the magnitude of  $C_{NL}$  is  
697 significantly and positively correlated with  $LAI_{NL}$ , accounting for over 50% of the inter-  
698 model variation in the C4MIP (**Fig. 13a**). Positive leaf-area nonlinearities ( $LAI_{NL}$ ) are closely  
699 tied to nonlinear changes in  $GPP_{NL}$  and by extension, to the carbon feedbacks (**Figs. 4-6**),  
700 suggesting the RAD-BGC interactions in carbon cycle processes amplify plant growth and  
701 consequent ET. We pool all model grid points together, bin them into their  $LAI_{NL}$  and  $C_{NL}$   
702 responses, and calculate the area-weighted average of  $\Delta(C/P)_{NL}$  across all model grid points  
703 falling in each  $LAI_{NL}$  and  $C_{NL}$  bin (**Fig. 13b, Methods**). Across spatial scales there is a clear  
704 positive correlation between nonlinear leaf area increases, nonlinear canopy water fluxes  
705 from plant-based ET, and nonlinear precipitation partitioning to plants (C/P). The positive  
706 association among all three is strong, suggesting that plant growth nonlinearities influence

707 both the relative and absolute increases in simulated ecosystem water use across models,  
 708 regions, climates, and biomes.



709

710 **Fig. 13** Linking plant greening to soil drying in the C4MIP. **a**, The inter-model association between the  
 711  $4xCO_2$  response in the nonlinear LAI term ( $LAI_{NL}$ , %) and the nonlinear canopy water flux term ( $C_{NL}$ , mm  
 712  $WY^{-1}$ ) over global land areas. **b**, The model-grid point association among  $LAI_{NL}$  term and  $C_{NL}$ . Colors  
 713 indicate area-weighted model-grid point average change in nonlinear canopy partitioning  $(C/P)_{NL}$   
 714 in percentage points (pp). **c**, The inter-model association among  $4xCO_2$  changes in total canopy throughfall,  
 715 calculated as the difference between WY precipitation and WY leaf evaporation ( $P-E_L$ , mm  $WY^{-1}$ ) and  
 716 total runoff (mm  $WY^{-1}$ ) in the COU run. **d**, As in **b**, except showing the model-grid point association  
 717 among precipitation throughfall, runoff, and runoff partitioning (colors) from the COU run. **e**, The inter-  
 718 model association among the  $C_{NL}$  (mm  $WY^{-1}$ ) and the nonlinear soil water flux ( $S_{NL}$ , mm  $WY^{-1}$ ). **f**, as in **b**  
 719 and **d**, but showing the model-grid point association between  $C_{NL}$  and  $S_{NL}$ . Colors indicate the nonlinear  
 720 soil partitioning,  $(S/P)_{NL}$ . In **a**, **c**, and **e**, R-squared and p-values are reported. Model numbers are the same  
 721 as presented in **Figure 4-6**. In **b**, **d**, and **e**, red text indicates the percentage of pooled model-grid points  
 722 falling into that quadrant.

723 In contrast to the canopy water flux from plant-based ET, there is little nonlinearity  
 724 that emerges in runoff efficiency or runoff itself, and—where it exists—it tends to be  
 725 negative or insignificant, implying that interactions among the RAD and BGC weakly reduce

726 runoff (e.g., **Figs. 9h, 12k-m**). Because there is not a strong nonlinear runoff term to explain,  
727 we instead focus on the factors determining total runoff in the fully-coupled COU run (**Fig.**  
728 **13c,d**). While the assumption has always been that plant-driven runoff enhancements were  
729 conditioned on precipitation changes, precipitation, not plants, is the dominant factor shaping  
730 runoff changes across the ensemble, even in the BGC run where plant effects are thought to  
731 be central to hydrologic changes (**Fig. 11-13**). Nonlinear vegetation responses do appear to  
732 shape runoff responses in regions with precipitation decreases, reducing runoff ratio or  
733 countering any runoff ratio gains from the BGC run (**Fig. 11f**, pink line). This implies that in  
734 the models, plants take their share of precipitation regardless of precipitation change, which  
735 in turn cuts into the runoff allocation where precipitation is limited. In contrast, runoff  
736 appears to increase primarily through increased precipitation (**Figs. 12e,l**) and canopy  
737 throughfall, with the latter estimated as the difference between precipitation and leaf  
738 evaporation (**Fig. 13c, d**).

739 The relationship between throughfall, runoff, and runoff partitioning is clear at both the  
740 inter-model and model grid-point scales, as enhanced throughfall increases runoff (**Figs. 13c,**  
741 **d**). As such, in regions where increased runoff efficiency does occur, these changes are  
742 associated with precipitation changes that more than compensate for canopy interception and  
743 leaf evaporation changes, or have larger increases in extreme precipitation relative to other  
744 regions (**Fig. S4**). For example, changes in extreme precipitation changes (defined as the  
745 maximum total precipitation (mm) occurring over a five-day period in each WY) in  $\Delta(Q/P)$   
746 positive regions are 50% larger than in  $\Delta(C/P)$  positive regions, driven by a strong radiative  
747 response in those regions (**Fig. S4d,e**). This is consistent with earlier work that showed that  
748 the strength of extreme precipitation change accounts for the strength of runoff efficiency  
749 changes in models (Mankin et al. 2018).

750 We find that plant changes due to interactions of the RAD and BGC runs act to draw  
751 down soil water, drying the surface (**Fig. 13e-f**). Global-scale inter-model decreases in the  
752 nonlinear soil term ( $S_{NL}$ ) are tightly associated with increases in the nonlinear canopy water  
753 flux term ( $C_{NL}$ ) (**Fig. 13e**). The result implies that the resultant increase in plant-based ET  
754 (e.g., **Fig. 13a,b**) comes at the expense of soil water. This relationship holds across grid  
755 points and models, as positive nonlinear canopy water use is associated with decreases in  
756 nonlinear soil partitioning,  $(S/P)_{NL}$  (colors in **Fig. 13f**). This implies that the strength of the  
757 greening and drying pattern in the CMIP6 ensemble (**Fig. 1**) is, in part, a function of the

758 nonlinear increase in plant growth and the associated increase in plant-based ET, which leads  
759 to soil water reductions in the CMIP6 ensemble.

#### 760 **4. Discussion & Conclusions**

761 Relative to the CMIP5, the latest generation of CMIP6 ESMs simulate larger interactions  
762 between the radiative and biogeochemical effects of [CO<sub>2</sub>] (Huang et al. 2022) (**Fig. 4**).  
763 There are a number of potential reasons for the growth in these interactions, from varied  
764 sophistication in nutrient cycling schemes, or mortality, disturbance, and succession, among  
765 others. Irrespective of the precise reasons for these emergent interactions between the  
766 radiative and biogeochemical effects of CO<sub>2</sub>, they lead to larger and more uncertain nonlinear  
767 terms in plant growth and net ecosystem exchange that are associated with a reduced  
768 sensitivity of the land carbon feedbacks to warming across the ensemble (**Fig. 5**). These plant  
769 nonlinearities have consequences for hydrology (**Figs. 8-13**): leaf areas increase beyond what  
770 would be predicted by the sum of CO<sub>2</sub> fertilization and radiative effects alone, leading to  
771 *increased* ecosystem water use, both absolutely (as total plant-based ET increases) (**Fig. 8**)  
772 and relatively (as plant-based ET comprises an increasing fraction of precipitation) (**Fig. 9**).  
773 These increases in plant-based ET from interactions among RAD and BGC contribute to  
774 land-surface drying (**Figs. 11-12**) or counter any gains from increased ecosystem WUE.  
775 Vegetation in these latest simulations only increases water availability when comparing  
776 radiative and biogeochemical simulations in isolation (Swann et al. 2016; Scheff et al. 2021).  
777 When radiative and biogeochemical responses can interact in simulations as they do in the  
778 real world, the models suggest that vegetation and its water use counter (or exceed) any  
779 increases in runoff or soil moisture from stomatal closure in the BGC runs. In the fully  
780 coupled simulations, plants and their responses to [CO<sub>2</sub>] generally dry the land.

781 These results suggest that the curious global pattern of vegetation greening and land  
782 surface drying (Mankin et al. 2017) projected by the models appear to be internally  
783 consistent, meaning that the soil drying is, in part, associated with enhanced greening (**Figs.**  
784 **1, 13**). It does not suggest, however, that they are reflective of what will occur in the real  
785 world. Future investigations should consider the set of processes governing carbon uptake  
786 and release by the land (**Fig. 6**), and how this has evolved across the CMIP5 to CMIP6  
787 ensemble resulting in a weaker climate-carbon feedback (**Fig. 5b**).

788 That there are nonlinear interactions among nutrient cycles and warming is not surprising  
789 given the long history of work on feedbacks and dynamics in the plant physiology, ecology,  
790 and nutrient cycle communities (Burkett et al. 2005; Field et al. 1995, 2007). It is also not  
791 surprising that the magnitude of and uncertainty in such interactions increase with model  
792 sophistication in representing these processes (Fisher and Koven 2020; Zaehle et al. 2015).  
793 However, the emergence of sizable nonlinear interactions in carbon feedbacks appears to be a  
794 new feature of the latest generation of CMIP relative to earlier generations (e.g., **Fig. 4**)  
795 (Huang et al. 2022). While new parameterizations likely make land surface schemes more  
796 reflective of real-world processes, how they interact to shape model responses and accuracy  
797 requires continued evaluation. Certainly, in this instance, the C4MIP range in the magnitude  
798 of nonlinear carbon responses has increased relative to CMIP5, and the reasons for this  
799 change are a worthy subject of future work.

800 Our findings reinforce a more widespread need for the perturbed parameter ensembles  
801 being pursued by researchers in the land surface modeling community (Zarakas et al. 2024;  
802 McNeall et al. 2024). As science seeks to understand the independent and interactive effects  
803 of these parametrizations schemes around plants, nutrients, and hydrology, such interactions  
804 can shape very different model answers, even within the same land surface model (Zarakas et  
805 al. 2020, 2024). Our results here emphasize a point relevant to these efforts: one-at-a-time  
806 perturbed parameter ensembles, while computationally feasible, may actually be insufficient  
807 to characterize the importance of any one land surface parameter, owing to interactive effects.  
808 Instead, “global variance-based” sensitivity analyses (Saltelli 2000; Saltelli et al. 2010)  
809 should be pursued, where modelers jointly and independently perturb carbon, plant, and  
810 water parameters to evaluate not just the contribution of any one parameter to the distribution  
811 of model answers, but how interactions among parameters shape uncertainties in model  
812 responses. These ensembles could help identify the parameters most culpable for uncertainty  
813 in RAD and BGC interactions and position their benchmarking to the real world.

814 Despite a remaining need to investigate the processes underpinning the uncertain carbon,  
815 plant, and water interactions across model generations, there are some key takeaways from  
816 our work. Most importantly, our results demonstrate that making plant water consumption  
817 assessments based on radiative or biogeochemical effects alone neglects a sizable interaction  
818 in the latest generation of models. Ignoring this interaction will lead to a misdiagnosis of the  
819 simulated drivers of the water balance and how that is shaped by nonlinear features in the

820 land carbon response to forcing. While some previous work on amplified runoff responses to  
821 plant physiological effects noted a small nonlinearity in the CMIP5 version of the C4MIP  
822 experiments or constrained their analyses to regions where such nonlinearity was small  
823 (Fowler et al. 2019), this nonlinear term has doubled in size for CMIP6 (**Fig. 4**). As such, in  
824 current model generations, independently comparing the responses in the RAD and BGC  
825 simulations can lead to the incorrect conclusion that plant responses to enhanced [CO<sub>2</sub>] yield  
826 a net wetting effect.

827 As ESMs incorporate more sophisticated processes (Fisher and Koven 2020),  
828 nonlinearities are emerging with hydrologic consequences. Furthermore, considerable  
829 uncertainties in land carbon and hydrology stem from model representations of phenology,  
830 nutrient limitations, soil microbial and respiratory processes, vegetation mortality from  
831 wildfire, insects and pathogens, drought stress, wind storms, and post-disturbance  
832 successional processes (Ziehn et al. 2021; Sanderson and Fisher 2020; Albrich et al. 2020;  
833 Trugman et al. 2018; Zaehle et al. 2015; Fisher and Koven 2020). To better represent the land  
834 carbon sink and its implications for water availability for people and ecosystems, model  
835 development is rightfully focused on improving representation of the soil water-plant-  
836 atmosphere continuum (Clark et al. 2015) and plant mortality and succession (Anderegg et al.  
837 2013; Trugman et al. 2018; Williams et al. 2022). To what extent these processes collectively  
838 generate nonlinear feedbacks in the real world is poorly understood and must be validated. At  
839 the same time, greater model sophistication may improve the realism of any one model, it  
840 may also give rise to additional poorly understood nonlinear feedbacks, which may, or may  
841 not, be reflective of the real world. Identification of these nonlinearities and their  
842 consequences, as we have done here, is an essential step and creates a scientific imperative to  
843 understand the genesis and validity of the emerging and pronounced nonlinearities in our  
844 state-of-the-art ESMs.

845

846 *Acknowledgments.*

847 We acknowledge the Earth System Grid Federation and their archiving of the Coupled  
848 Model Intercomparison Project (Phase 6) data. We thank Dartmouth's Research Computing,  
849 which provided computational support, as well as Naomi Henderson and H. Liu for data  
850 serving support in the Division of Ocean and Climate Physics at Lamont-Doherty Earth  
851 Observatory of Columbia University. We thank Y. Huang (CSIRO) and V. Arora (CCMA) for

852 sharing additional details of the feedback parameter calculations. We thank two reviewers  
853 (including V. Arora) for their contributions to improving this work, as well as the participants  
854 of the Carnegie Trust-funded workshop on “Continental Climate Change: Simple Models to  
855 Understand the Future” held at University of St. Andrews for providing feedback on this work.  
856 We acknowledge funding from NOAA MAPP NA20OAR4310425 (J.S.M, R.S., J.E.S., and  
857 Z.L); DOE DESC0022302 (J.S.M, B.I.C, R.S., A.P.W. and J.E.S.); FRQNT 31916 (C. L.);  
858 NSF CLD 2304953 (J.S.M); the Gordon and Betty Moore Foundation 11974 (A.P.W.); and the  
859 Neukom Institute for Computational Science (J.S.M., C.L., and E.D.M.) and the Rockefeller  
860 Center at Dartmouth (J.S.M.).

861

#### 862 *Data Availability Statement.*

863 All CMIP5 and CMIP6 C4MIP data that support this study are publicly available at:  
864 <https://esgf-node.llnl.gov/>. All code that supports this study will be made available upon  
865 reasonable request.

866

867

#### REFERENCES

868 Albrich, K., W. Rammer, M. G. Turner, Z. Ratajczak, K. H. Braziunas, W. D. Hansen, and R.  
869 Seidl, 2020: Simulating forest resilience: A review. *Global Ecology and*  
870 *Biogeography*, **29**, 2082–2096, <https://doi.org/10.1111/geb.13197>.

871 Anderegg, W. R. L., J. Kane, and L. D. L. Anderegg, 2013: Consequences of widespread tree  
872 mortality triggered by drought and temperature stress. *Nature Climate Change*, **3**, 30–  
873 30, <https://doi.org/10.1038/NCLIMATE1635>.

874 Arora, V. K., and Coauthors, 2020: Carbon–concentration and carbon–climate feedbacks in  
875 CMIP6 models and their comparison to CMIP5 models. *Biogeosciences*, **17**, 4173–  
876 4222, <https://doi.org/10.5194/bg-17-4173-2020>.

877 Aston, A. R., 1984: The effect of doubling atmospheric CO<sub>2</sub> on streamflow: A simulation.  
878 *Journal of Hydrology*, **67**, 273–280, [https://doi.org/10.1016/0022-1694\(84\)90246-4](https://doi.org/10.1016/0022-1694(84)90246-4).

879 Betts, R. A., and Coauthors, 2007: Projected increase in continental runoff due to plant  
880 responses to increasing carbon dioxide. *Nature*, **448**, 1037–1041,  
881 <https://doi.org/10.1038/nature06045>.

882 Bonan, G. B., M. Williams, R. A. Fisher, and K. W. Oleson, 2014: Modeling stomatal  
883 conductance in the earth system: linking leaf water-use efficiency and water transport  
884 along the soil–plant–atmosphere continuum. *Geoscientific Model Development*, **7**,  
885 2193–2222, <https://doi.org/10.5194/gmd-7-2193-2014>.

- 886 Burkett, V. R., and Coauthors, 2005: Nonlinear dynamics in ecosystem response to climatic  
887 change: Case studies and policy implications. *Ecological Complexity*, **2**, 357–394,  
888 <https://doi.org/10.1016/j.ecocom.2005.04.010>.
- 889 Canadell, J.G., Monteiro, P.M.S., Costa, M.H., Cotrim da Cunha, L., Cox, P.M., Eliseev,  
890 A.V., Henson, S., and Ishii, M., 2021: Global Carbon and other Biogeochemical  
891 Cycles and Feedbacks. *Climate Change 2021: The Physical Science Basis. Contribution of Working Group I to the Sixth Assessment Report of the Intergovernmental Panel on Climate Change [Masson-Delmotte, V., P. Zhai, A. Pirani, S.L. Connors, C. Péan, S. Berger, N. Caud, Y. Chen, L. Goldfarb, M.I. Gomis, M. Huang, K. Leitzell, E. Lonnoy, J.B.R. Matthews, T.K. Maycock, T. Waterfield, O. Yelekçi, R. Yu, and B. Zhou (eds.)]*. doi: 10.1017/9781009157896.007, Cambridge University Press, 673-816,.
- 898 Clark, M. P., and Coauthors, 2015: Improving the representation of hydrologic processes in  
899 Earth System Models. *Water Resources Research*, **51**, 5929–5956,  
900 <https://doi.org/10.1002/2015WR017096>.
- 901 Cook, B. I., J. S. Mankin, K. Marvel, A. P. Williams, J. E. Smerdon, and K. J. Anchukaitis,  
902 2020: Twenty-First Century Drought Projections in the CMIP6 Forcing Scenarios.  
903 *Earth's Future*, **8**, e2019EF001461, <https://doi.org/10.1029/2019EF001461>.
- 904 ———, ———, A. P. Williams, K. D. Marvel, J. E. Smerdon, and H. Liu, 2021: Uncertainties,  
905 Limits, and Benefits of Climate Change Mitigation for Soil Moisture Drought in  
906 Southwestern North America. *Earth's Future*, **9**, e2021EF002014,  
907 <https://doi.org/10.1029/2021EF002014>.
- 908 Cowan, I. R., and G. D. Farquhar, 1977: Stomatal function in relation to leaf metabolism and  
909 environment. *Integration of Activity in the Higher Plant*, Cambridge University Press,  
910 p. 18.
- 911 Cox, P. M., D. Pearson, B. B. Booth, P. Friedlingstein, C. Huntingford, C. D. Jones, and C.  
912 M. Luke, 2013: Sensitivity of tropical carbon to climate change constrained by carbon  
913 dioxide variability. *Nature*, **494**, 341–344, <https://doi.org/10.1038/nature11882>.
- 914 Davies-Barnard, T., and Coauthors, 2020: Nitrogen cycling in CMIP6 land surface models:  
915 progress and limitations. *Biogeosciences*, **17**, 5129–5148, <https://doi.org/10.5194/bg-17-5129-2020>.
- 917 De Kauwe, M. G., and Coauthors, 2013: Forest water use and water use efficiency at elevated  
918 CO<sub>2</sub>: A model-data intercomparison at two contrasting temperate forest FACE sites.  
919 *Global Change Biology*, **19**, 1759–1779, <https://doi.org/10.1111/gcb.12164>.
- 920 Eyring, V., S. Bony, G. A. Meehl, C. A. Senior, B. Stevens, R. J. Stouffer, and K. E. Taylor,  
921 2016: Overview of the Coupled Model Intercomparison Project Phase 6 (CMIP6)  
922 experimental design and organization. *Geoscientific Model Development*, **9**, 1937–  
923 1958, <https://doi.org/10.5194/gmd-9-1937-2016>.
- 924 Felzer, B. S., T. W. Cronin, J. M. Melillo, D. W. Kicklighter, and C. A. Schlosser, 2009:  
925 Importance of carbon-nitrogen interactions and ozone on ecosystem hydrology during

- 926 the 21st century. *Journal of Geophysical Research: Biogeosciences*, **114**,  
927 <https://doi.org/10.1029/2008JG000826>.
- 928 Field, C. B., R. B. Jackson, and H. A. Mooney, 1995: Stomatal responses to increased CO<sub>2</sub>:  
929 implications from the plant to the global scale. *Plant, Cell & Environment*, **18**, 1214–  
930 1225, <https://doi.org/10.1111/j.1365-3040.1995.tb00630.x>.
- 931 Field, C. B., D. B. Lobell, H. A. Peters, and N. R. Chiariello, 2007: Feedbacks of Terrestrial  
932 Ecosystems to Climate Change. *Annual Review of Environment and Resources*, **32**, 1–  
933 29, <https://doi.org/10.1146/annurev.energy.32.053006.141119>.
- 934 Fisher, R. A., and C. D. Koven, 2020: Perspectives on the Future of Land Surface Models  
935 and the Challenges of Representing Complex Terrestrial Systems. *Journal of*  
936 *Advances in Modeling Earth Systems*, **12**, e2018MS001453,  
937 <https://doi.org/10.1029/2018MS001453>.
- 938 Fowler, M. D., G. J. Kooperman, J. T. Randerson, and M. S. Pritchard, 2019: The effect of  
939 plant physiological responses to rising CO<sub>2</sub> on global streamflow. *Nature Climate*  
940 *Change*, **9**, 873–879, <https://doi.org/10.1038/s41558-019-0602-x>.
- 941 Friedlingstein, P., and Coauthors, 2006: Climate-Carbon Cycle Feedback Analysis: Results  
942 from the C4MIP Model Intercomparison. *Journal of Climate*, **19**, 3337–3353.
- 943 Fung, Inez, Rayner, Peter, and Friedlingstein, Pierre, 2000: Full-Form Earth System Models:  
944 Coupled Carbon-Climate Interaction Experiment (the “Flying Leap”). *IGBP*  
945 *Newsletter*, **41**.
- 946 Gottlieb, A. R., and J. S. Mankin, 2024: Evidence of human influence on Northern  
947 Hemisphere snow loss. *Nature*, **625**, 293–300, [https://doi.org/10.1038/s41586-023-](https://doi.org/10.1038/s41586-023-06794-y)  
948 [06794-y](https://doi.org/10.1038/s41586-023-06794-y).
- 949 Hall, A., P. Cox, C. Huntingford, and S. Klein, 2019: Progressing emergent constraints on  
950 future climate change. *Nature Climate Change*, **9**, 269–278,  
951 <https://doi.org/10.1038/s41558-019-0436-6>.
- 952 Huang, Y., Y.-P. Wang, and T. Ziehn, 2022: Nonlinear interactions of land carbon cycle  
953 feedbacks in Earth System Models. *Global Change Biology*, **28**, 296–306,  
954 <https://doi.org/10.1111/gcb.15953>.
- 955 Idso, S. B., and A. J. Brazel, 1984: Rising atmospheric carbon dioxide concentrations may  
956 increase streamflow. *Nature*, **312**, 51–53, <https://doi.org/10.1038/312051a0>.
- 957 Jasechko, S., 2018: Plants turn on the tap. *Nature Clim Change*, **8**, 562–563,  
958 <https://doi.org/10.1038/s41558-018-0212-z>.
- 959 Jones, C. D., and Coauthors, 2016: C4MIP-The Coupled Climate-Carbon Cycle Model  
960 Intercomparison Project: Experimental protocol for CMIP6. *Geoscientific Model*  
961 *Development*, **9**, 2853–2880, <https://doi.org/10.5194/gmd-9-2853-2016>.
- 962 Keenan, D. Y. Hollinger, G. Bohrer, D. Dragoni, J. W. Munger, H. P. Schmid, and A. D.  
963 Richardson, 2013: Increase in forest water-use efficiency as atmospheric carbon

- 964 dioxide concentrations rise. *Nature*, **499**, 324–327,  
965 <https://doi.org/10.1038/nature12291>.
- 966 Keenan, T. F., and Coauthors, 2023: A constraint on historic growth in global photosynthesis  
967 due to rising CO<sub>2</sub>. *Nat. Clim. Chang.*, **13**, 1376–1381,  
968 <https://doi.org/10.1038/s41558-023-01867-2>.
- 969 Lee, E., B. S. Felzer, and Z. Kothavala, 2013: Effects of nitrogen limitation on hydrological  
970 processes in CLM4-CN. *Journal of Advances in Modeling Earth Systems. Model.*  
971 *Earth Syst*, **5**, 741–754, <https://doi.org/10.1002/jame.20046>.
- 972 Lehner, F., A. W. Wood, J. A. Vano, D. M. Lawrence, M. P. Clark, and J. S. Mankin, 2019:  
973 The potential to reduce uncertainty in regional runoff projections from climate  
974 models. *Nature Climate Change*, **9**, 926–933, <https://doi.org/10.1038/s41558-019-0639-x>.
- 976 Lemordant, L., P. Gentine, A. S. Swann, B. I. Cook, and J. Scheff, 2018: Critical impact of  
977 vegetation physiology on the continental hydrologic cycle in response to increasing  
978 CO<sub>2</sub>. *Proceedings of the National Academy of Sciences*, **0**, 2–7,  
979 <https://doi.org/10.1073/pnas.1720712115>.
- 980 Leung, and Coauthors, 2023: Ch. 3. Earth systems processes. *Fifth National Climate*  
981 *Assessment*. Crimmins, A.R., C.W. Avery, D.R. Easterling, K.E. Kunkel, B.C. Stewart,  
982 and T.K. Maycock, Eds. U.S. Global Change Research Program, Washington, DC,  
983 USA. <https://doi.org/10.7930/NCA5.2023.CH3>, U.S. Global Change Research  
984 Program, Washington, DC, 1–470.
- 985 Liu, L., P. Ciais, M. Wu, R. S. Padrón, P. Friedlingstein, J. Schwaab, L. Gudmundsson, and  
986 S. I. Seneviratne, 2023: Increasingly negative tropical water–interannual CO<sub>2</sub> growth  
987 rate coupling. *Nature*, **618**, 755–760, <https://doi.org/10.1038/s41586-023-06056-x>.
- 988 Mankin, J. S., J. E. Smerdon, B. I. Cook, A. P. Williams, and R. Seager, 2017: The curious  
989 case of projected Twenty-First-Century Drying but Greening in the American West.  
990 *Journal of Climate*, **30**, 8689–8710, <https://doi.org/10.1175/JCLI-D-17-0213.1>.
- 991 ———, R. Seager, J. E. Smerdon, B. I. Cook, A. P. Williams, and R. M. Horton, 2018: Blue  
992 Water Trade-Offs With Vegetation in a CO<sub>2</sub>-Enriched Climate. *Geophysical*  
993 *Research Letters*, **45**, 3115–3125, <https://doi.org/10.1002/2018GL077051>.
- 994 ———, ———, ———, ———, and ———, 2019: Mid-latitude freshwater availability reduced by  
995 projected vegetation responses to climate change. *Nature Geoscience*,  
996 <https://doi.org/10.1038/s41561-019-0480-x>.
- 997 McNeall, D., E. Robertson, and A. Wiltshire, 2024: Constraining the carbon cycle in JULES-  
998 ES-1.0. *Geoscientific Model Development*, **17**, 1059–1089,  
999 <https://doi.org/10.5194/gmd-17-1059-2024>.
- 1000 Medlyn, B. E., and Coauthors, 2011: Reconciling the optimal and empirical approaches to  
1001 modelling stomatal conductance. *Global Change Biology*, **17**, 2134–2144,  
1002 <https://doi.org/10.1111/j.1365-2486.2010.02375.x>.

- 1003 Milly, P. C. D., and K. A. Dunne, 2016: Potential evapotranspiration and continental drying.  
1004 *Nature Climate Change*, **6**, 946–949, <https://doi.org/10.1038/NCLIMATE3046>.
- 1005 Roderick, M. L., P. Greve, and G. D. Farquhar, 2015: On the assessment of aridity with  
1006 changes in atmospheric CO<sub>2</sub>. *Water Resources Research*, **51**, 5450–5463,  
1007 <https://doi.org/10.1002/2015WR017031>.
- 1008 Sabot, M. E. B., and Coauthors, 2022: One Stomatal Model to Rule Them All? Toward  
1009 Improved Representation of Carbon and Water Exchange in Global Models. *Journal*  
1010 *of Advances in Modeling Earth Systems*, **14**, e2021MS002761,  
1011 <https://doi.org/10.1029/2021MS002761>.
- 1012 Saltelli, A., 2000: What is Sensitivity Analysis? *Sensitivity Analysis*, 3–13.
- 1013 ———, P. Annoni, I. Azzini, F. Campolongo, M. Ratto, and S. Tarantola, 2010: Variance based  
1014 sensitivity analysis of model output. Design and estimator for the total sensitivity  
1015 index. *Computer Physics Communications*, **181**, 259–270,  
1016 <https://doi.org/10.1016/j.cpc.2009.09.018>.
- 1017 Sanderson, B. M., and R. A. Fisher, 2020: A fiery wake-up call for climate science. *Nat.*  
1018 *Clim. Chang.*, **10**, 175–177, <https://doi.org/10.1038/s41558-020-0707-2>.
- 1019 Scheff, J., J. S. Mankin, S. Coats, and H. Liu, 2021: CO<sub>2</sub>-plant effects do not account for the  
1020 gap between dryness indices and projected dryness impacts in CMIP6 or CMIP5.  
1021 *Environmental Research Letters*, **16**, 034018, [https://doi.org/10.1088/1748-](https://doi.org/10.1088/1748-9326/abd8fd)  
1022 [9326/abd8fd](https://doi.org/10.1088/1748-9326/abd8fd).
- 1023 Skinner, C. B., and Coauthors, 2017: The role of plant CO<sub>2</sub> physiological forcing in shaping  
1024 future daily-scale precipitation. *Journal of Climate*, JCLI-D-16-0603.1,  
1025 <https://doi.org/10.1175/JCLI-D-16-0603.1>.
- 1026 Sokolov, A. P., D. W. Kicklighter, J. M. Melillo, B. S. Felzer, C. A. Schlosser, and T. W.  
1027 Cronin, 2008: Consequences of Considering Carbon–Nitrogen Interactions on the  
1028 Feedbacks between Climate and the Terrestrial Carbon Cycle. *Journal of Climate*, **21**,  
1029 3776–3796, <https://doi.org/10.1175/2008JCLI2038.1>.
- 1030 Swann, A. L. S., F. M. Hoffman, C. D. Koven, and J. T. Randerson, 2016: Plant responses to  
1031 increasing CO<sub>2</sub> reduce estimates of climate impacts on drought severity. *Proceedings*  
1032 *of the National Academy of Sciences*, **113**, 10019–10024,  
1033 <https://doi.org/10.1073/pnas.1604581113>.
- 1034 Thornton, P. E., and Coauthors, 2009: Carbon-nitrogen interactions regulate climate-carbon  
1035 cycle feedbacks: results from an atmosphere–ocean general circulation model.  
1036 *Biogeosciences*, **6**, 2099–2120, <https://doi.org/10.5194/bg-6-2099-2009>.
- 1037 Trugman, A. T., D. Medvigy, J. S. Mankin, and W. R. L. L. Anderegg, 2018: Soil moisture  
1038 drought as a major driver of carbon cycle uncertainty. *Geophysical Research Letters*,  
1039 **45**, 6495–6503, <https://doi.org/10.1029/2018GL078131>.
- 1040 Vitousek, P. M., and R. W. Howarth, 1991: Nitrogen limitation on land and in the sea: How  
1041 can it occur? *Biogeochemistry*, **13**, 87–115, <https://doi.org/10.1007/BF00002772>.

- 1042 Wenzel, S., P. M. Cox, V. Eyring, and P. Friedlingstein, 2014: Emergent constraints on  
1043 climate-carbon cycle feedbacks in the CMIP5 Earth system models. *Journal of*  
1044 *Geophysical Research: Biogeosciences*, **119**, 794–807,  
1045 <https://doi.org/10.1002/2013JG002591>.Received.
- 1046 Williams, A. P., and Coauthors, 2022: Growing impact of wildfire on western US water  
1047 supply. *PNAS*, **119**, <https://doi.org/10.1073/pnas.2114069119>.
- 1048 Yang, Y., M. L. Roderick, S. Zhang, T. R. Mcvicar, and R. J. Donohue, 2019: Hydrologic  
1049 implications of vegetation response to elevated CO<sub>2</sub> in climate projections. *Nature*  
1050 *Climate Change*, **9**, 44–49, <https://doi.org/10.1038/s41558-018-0361-0>.
- 1051 Zaehle, S., 2013: Terrestrial nitrogen–carbon cycle interactions at the global scale.  
1052 *Philosophical Transactions of the Royal Society B: Biological Sciences*, **368**,  
1053 20130125, <https://doi.org/10.1098/rstb.2013.0125>.
- 1054 Zaehle, S., P. Friedlingstein, and A. D. Friend, 2010: Terrestrial nitrogen feedbacks may  
1055 accelerate future climate change. *Geophysical Research Letters*, **37**, L01401,  
1056 <https://doi.org/10.1029/2009GL041345>.
- 1057 ———, C. D. Jones, B. Houlton, J.-F. Lamarque, and E. Robertson, 2015: Nitrogen  
1058 Availability Reduces CMIP5 Projections of Twenty-First-Century Land Carbon  
1059 Uptake. *Journal of Climate*, **28**, 2494–2511, <https://doi.org/10.1175/JCLI-D-13-00776.1>.
- 1061 Zarakas, C. M., A. L. S. Swann, M. M. Laguë, K. C. Armour, and J. T. Randerson, 2020:  
1062 Plant Physiology Increases the Magnitude and Spread of the Transient Climate  
1063 Response to CO<sub>2</sub> in CMIP6 Earth System Models. *Journal of Climate*, **33**, 8561–  
1064 8578, <https://doi.org/10.1175/JCLI-D-20-0078.1>.
- 1065 Zarakas, C. M., and Coauthors, 2024: Land Processes Can Substantially Impact the Mean  
1066 Climate State.
- 1067 Zhang, J., and Coauthors, 2018: Insights into the Molecular Mechanisms of CO<sub>2</sub>-Mediated  
1068 Regulation of Stomatal Movements. *Current Biology*, **28**, R1356–R1363,  
1069 <https://doi.org/10.1016/j.cub.2018.10.015>.
- 1070 Zhou, S., B. Yu, B. R. Lintner, K. L. Findell, and Y. Zhang, 2023: Projected increase in  
1071 global runoff dominated by land surface changes. *Nat. Clim. Chang.*, 1–8,  
1072 <https://doi.org/10.1038/s41558-023-01659-8>.
- 1073 Ziehn, T., Y.-P. Wang, and Y. Huang, 2021: Land carbon-concentration and carbon-climate  
1074 feedbacks are significantly reduced by nitrogen and phosphorus limitation. *Environ.*  
1075 *Res. Lett.*, **16**, 074043, <https://doi.org/10.1088/1748-9326/ac0e62>.
- 1076

**Supplemental Material:**

**Nonlinear carbon feedbacks in CMIP6 and their impacts on future  
freshwater availability**

Justin S. Mankin<sup>a,b</sup>, Noel Siegert<sup>a,b</sup>, Jason E. Smerdon<sup>b,c</sup>, Benjamin I. Cook<sup>b,d</sup>, Richard Seager<sup>b</sup>,  
A. Park Williams<sup>e</sup>, Corey Lesk<sup>a</sup>, Zhiying Li<sup>a</sup>, Harmanveer Singh<sup>a,f</sup>, & Emily Martinez<sup>a</sup>

<sup>a</sup> *Department of Geography, Dartmouth College, Hanover, NH*

<sup>b</sup> *Lamont-Doherty Earth Observatory of Columbia University, Palisades, NY*

<sup>c</sup> *Columbia Climate School, Columbia University, New York, NY*

<sup>d</sup> *NASA Goddard Institute for Space Studies, New York, NY*

<sup>e</sup> *Department of Geography, UCLA, Los Angeles, CA*

<sup>f</sup> *School of Marine & Atmospheric Sciences, Stony Brook University, Stony Brook, NY*

**This is a preprint, resubmitted to *Journal of Climate***

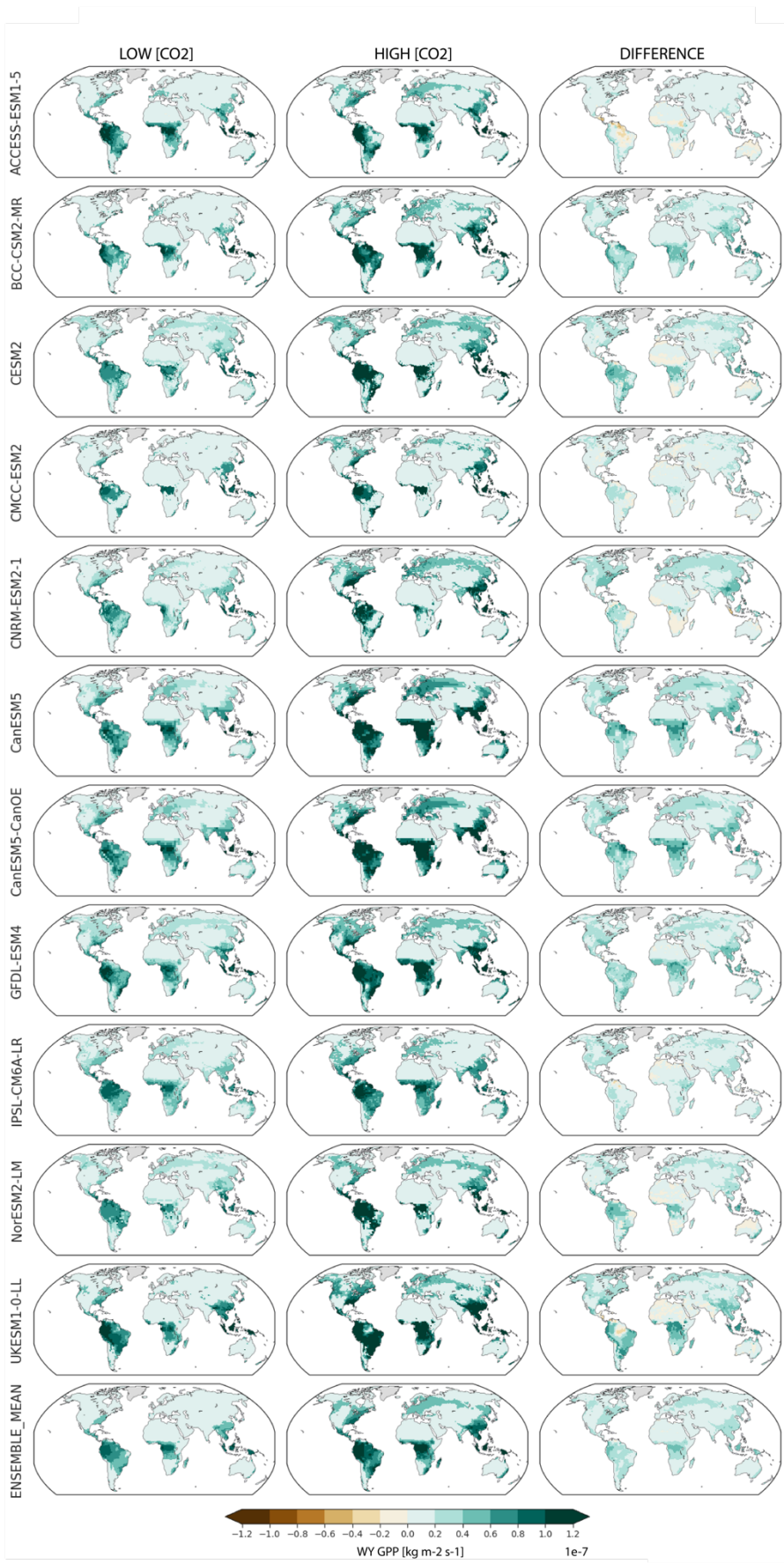


**Fig. S1** Climatological GPP and its change in the 1pctCO2 fully coupled simulation (COU) for each model in the analysis and the ensemble mean (rows). Columns correspond to the climatological water-year (WY) mean of GPP in the first 30 years, last 30 years, and difference among the two periods for each simulation.

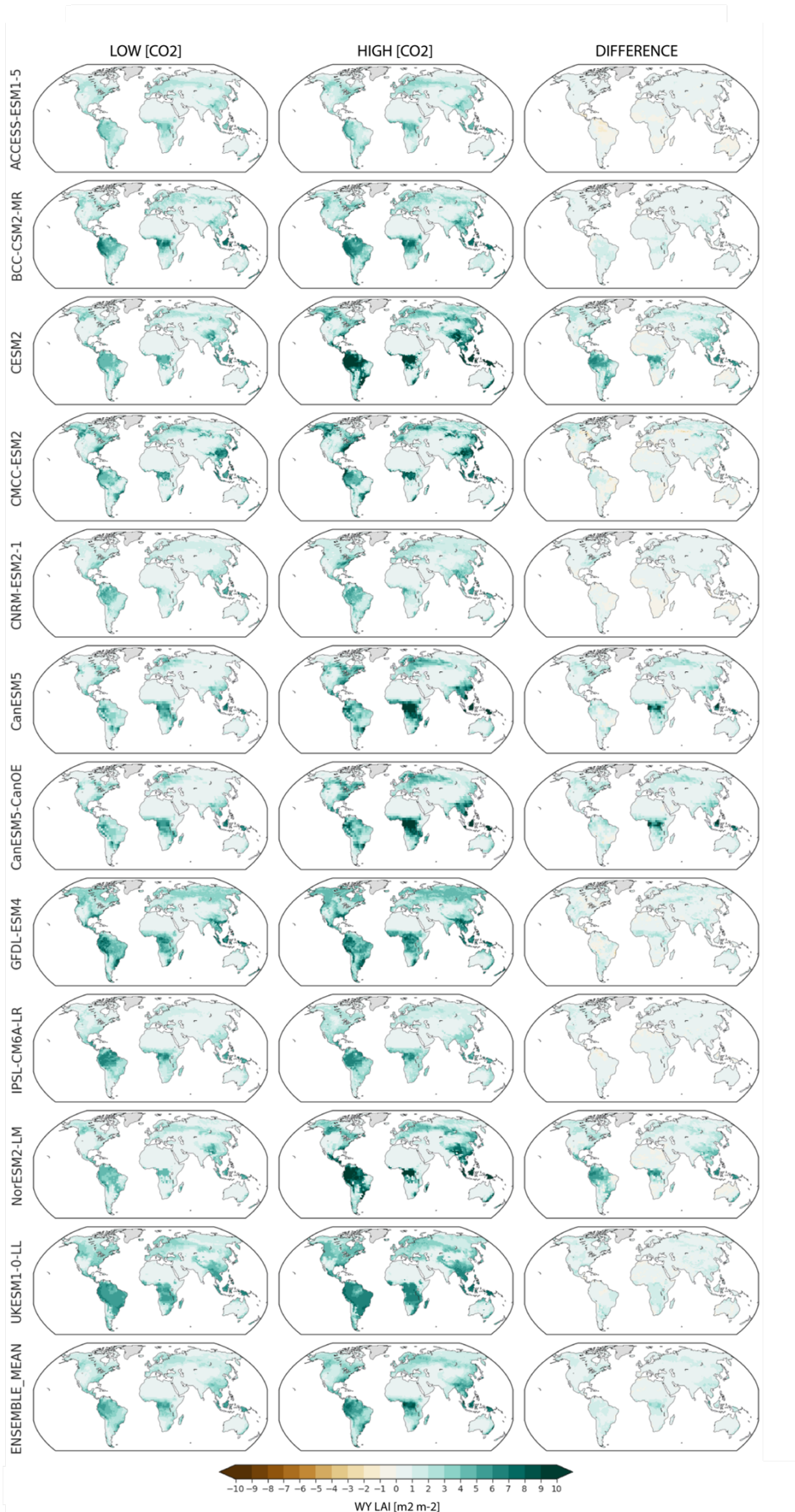


**Fig. S2** Climatological LAI and its change in the 1pctCO2 fully coupled simulation (COU) for each model in the analysis and the ensemble mean (rows). Columns correspond to the climatological water-year (WY) mean of LAI in the first 30 years, last 30 years, and difference among the two periods for each simulation.

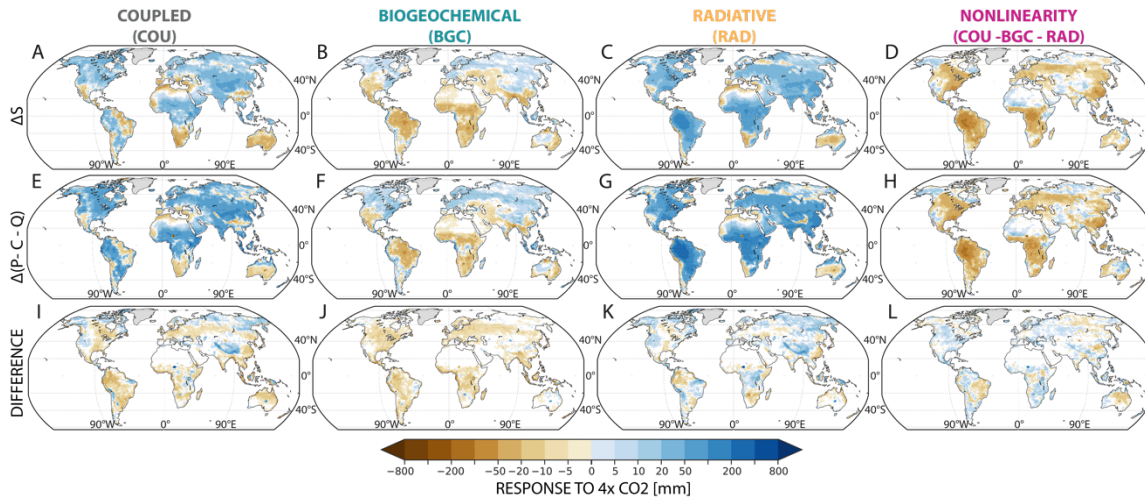


**Fig. S3** Climatological water-year (WY) changes in response to 4xCO<sub>2</sub> in the S term used in the analysis, defined as the sum of soil evaporation and the first difference of 2-m soil moisture (**a-d**), versus the S term when it is calculated as the residual of the difference between P, C, and Q (**e-h**). The last row (**i-l**) shows the difference between the two estimates of the S term.

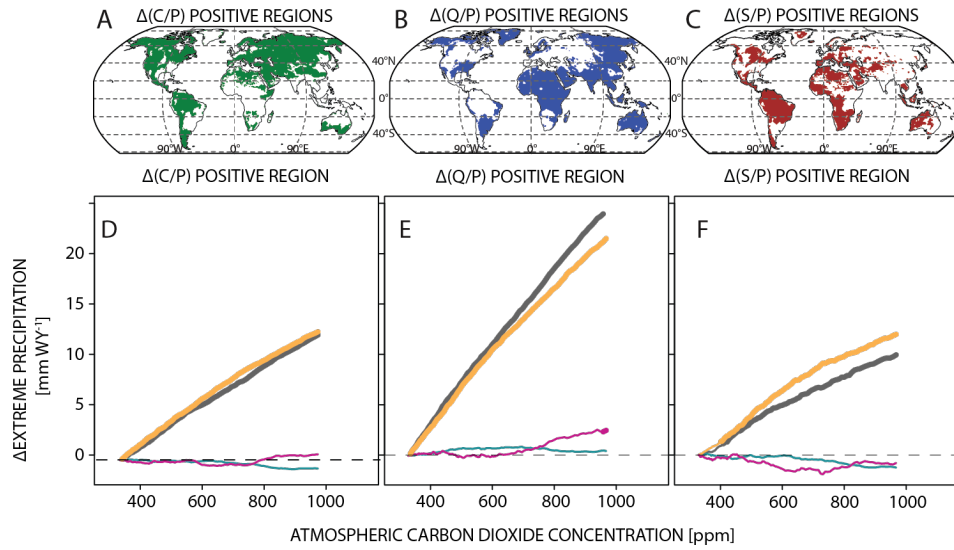


**Fig. S4** Changes in extreme precipitation (**d-f**) as a function of increasing [CO<sub>2</sub>] in Δ(C/P), Δ(Q/P), and Δ(S/P) regions (**a-c**) based on the COU run (see maps in **Fig. 9, a, e, i**). Significance in the time series is presented as a bolded line where the 30-year rolling ensemble mean change is greater than one standard deviation of changes across the ensemble at that time.